Action Potential Initiation in a Damaged Axon Initial Segment

by Louis Jacques

A thesis submitted to
the Faculty of Graduate Studies and Research
in partial fulfillment of the requirements for the
M.Sc. in Physics

Department of Physics
University of Ottawa

Contents

List of Figures

Abstract

We constructed a model for the initiation of the action potential (AP) in a damaged axon initial segment(AIS). We modelled the full axon including the AIS with a system of partial differential equations that we solved numerically. The damage was modelled on the AIS by having selected voltage-gated sodium channels affected by a coupled left-shift (CLS) of their activation and inactivation gating dynamics. We found that increased CLS lowered the threshold of spike initiation. We also found that CLS decreased the delay of spike initiation, especially for longer AIS. We also found that variability in the initiation timing increased with CLS. We also explored the effect of the geometry of the AIS on the initiation, finding that decreasing the radius favoured the initiation in the distal part of the AIS.

Acknowledgments

I would like to express my deepest gratitude to my supervisors, Dr Béla Joós and Dr André Longtin, for their patience and support in this projet. I would also like to thank Dr Catherine Morris for the invaluable insights in this field. I acknowledge financial support from NSERC through its CREATE training program in Quantitative Biomedicine held at the University of Ottawa.

Chapter 1

Introduction

The incidence of brain injuries in the population is very high. Such injuries usually have long lasting effects on the victims. Further, the brain is the most difficult organ to treat as it mostly does not regenerate, can't be transplanted, and neurosurgeries are delicate and risky. Brain injuries range from the most traumatic types such as penetrating head injuries, to the more benign yet painfully pervasive concussions. They also include non-traumatic injuries such as stroke and tumours. The symptoms of some of these injuries are such that they make differential diagnosis difficult. For example, the tests for identifying a stroke in the cerebellum and a drunk driver are very similar. Depressive-symptoms can hide a concussion. A focussed injury impairing speech and concentration will be unconsciously compensated by social isolation. Regardless of the cause, those symptoms are in themselves debilitating, but the danger of missed or delayed diagnosis of brain injuries, even the mildest, lies in what can follow when untreated: the secondary injuries. They follow the primary injuries while the ill-prepared brain is reacting to the situation.

The nervous tissues spend most of their energy in maintaining homeostasis, an out-of-equilibrium steady state of ion concentrations and protein distributions. This state relies on a complex and entangled network of interactions involving many structures, proteins and biophysical mechanisms. The disruption of one element in this network can lead to a cascade of changes, eventually throwing the whole system off balance. The diffuse axonal injuries occur when high accelerations create shearing forces throughout the brain. In moderate cases, when neurons aren't teared, the direct injury affects the internal protein skeleton of

the cells, known as the cytoskeleton, by partially unsticking it from the membrane in few places. However, the symptoms can be still be severe as this cytoskeleton disruption leads to calcium ions invading the cell. This in turn brings on an abnormal level of enzymatic reactions that degrade vital cellular structures, which eventually triggers apoptosis, i.e. cell death.

In milder cases like concussions, when this cascade stops before this calcium-led tipping point, other secondary injuries can have significant effects. There is evidence that the calcium invasion is caused by disrupted sodium channels, now disconnected from the cytoskeleton. Sodium channels are not only important for homeostasis, they are the heart of the primary function of each neuron: action potential generation, also known as spiking or firing. Action potentials are electrochemical waves that are initiated and propagated nonlinearly to other neurons where they are responsible for the release of neurotransmitter. Even if the damage to sodium channels is not enough to disrupt homeostasis, can it still affect its spiking properties significantly? In this thesis, we will explore a facet of this question, specifically, how damaged sodium channels affects the voltage threshold and temporal delay for the initiation of action potentials in the axon initial segment (AIS). This specialized structure on the neuron, which actually sits between the cell body ("soma") and the axon, is a highly sensitive zone that determines when the electrical currents from the soma, pooled from interactions with other cells, yield an action potential.

This initiation site of action potentials (aka spikes) is particularly sensitive to damage. Diffuse axonal injuries have been found to mostly affect the region between the grey and white matter, which are mainly composed, respectively, of somas and axons wrapped in a fatty insulating protein known as myelin. As the AIS lies between the soma and the rest of the axon, it is a likely target of injuries. It has also been shown that the AIS reacts more strongly to ischemic injuries (deprivation of fresh blood supply). One other important aspect of the AIS is its very unique organization of the sodium channels. This makes the AIS a prime target for sodium channel pathologies.

The initiation of the action potential is of interest as it is a primary function of the AIS and it happens on a time scale well separated from other processes that follow the injury, i.e. in milliseconds compared to seconds, minutes, hours and even days. The unique organization

of the AIS into two specific types of sodium channels, one low threshold and the other high, and one close to the soma and the other to the axon, is puzzling. This question is addressed in this thesis, in particular how this organization renders the neuron robust to mild damage to its sodium channels. We present a new model combining the geometry of the axon and the change in the kinetics of damaged voltage-gated sodium channels.

This thesis is presented in four parts. We first present the papers that motivated this investigation. We then present an introduction to the biology involved to ground the modeling effort in biophysical reality. In the next part the theoretical biophysical model of the AIS is constructed based on our biological understanding. Finally, the last part uses the model to numerically simulate the initiation of spikes in the AIS and its reaction to damaged sodium channels.

Chapter 2

Background

Our modeling study of the effect of damaged sodium channels in the axon initial segment (AIS) was motivated by recent papers that highlight the importance of sodium channel dynamics in this specialized section of the neuron. Two points stand out: 1) the AIS is highly specialized and organized in its molecular makeup and its functions, and 2) the AIS is very sensitive to injury. Those studies are summarized below and provide much of the research context for the rest of the thesis. The concepts described here will also be further explained in the following chapters.

2.1 Previous experimental studies

2.1.1 On the Coupled Left-Shifted sodium channels

[Wang et al., 2009]

In this experiment, the authors damaged in a well-defined manner a specific subtype of sodium channels and recorded their gating dynamics. They tested the hypothesis that sodium channels were at the origin of the calcium overload in stretched membrane. By inducing membrane blebbing, i.e. protrusions of the plasma membrane, they found that the sodium channels behaved abnormally. Their gating mechanism was modified in such a way that their current at rest was higher. This was due to a leftward shift (i.e. to more negative intracellular voltages with respect to the exterior of the cell) in the voltage dependence of

the gating mechanism. This is the case for both the so-called activation and inactivation parts of the gating mechanism, which will be detailed in chapter 4. This coupled-left-shift (CLS) result is an important key to understanding many effects of damage on neurons. It has motivated well-defined numerical studies of the consequences of such damaged membrane to spike initiation and propagation. It allow focusses studies of possible therapeutic solutions that avoid secondary degeneration caused by calcium overload in brain trauma victims.

2.1.2 On the dysruption of the AIS cytoskeleton

[Schafer et al., 2009]

This experiment looked at the effect on the axon initial segments of cutting the blood supply, i.e. an ischemic injury, in a region of mouse brain. They observed that the cytoskeleton of the AIS was the preferentially damaged part of the axon compared to the nodes of Ranvier. They analysed the by-products left after the injury to reconstruct the injury mechanism, and found that the calcium-dependent protease calpain was responsable for the degeneration of the cytoskeleton. This is again a link between injury and calcium overload. From this study we understood that sodium channel damage, already linked to cytoskeleton disruption, would have more effect on the AIS.

2.1.3 On the density of sodium channels in the AIS

[Lorincz and Nusser, 2010]

Despite the paper's title '*Molecular identity of dendritic voltage-gated sodium channels*', this study gave in unprecedented detail the density of sodium channels in the AIS. They used an immunogold labeling method, which uses gold particles attached to antibodies specific to sodium channel types. These gold particles appear as clear dots under an electron microscope. They studied the AIS only as a point of comparison for the densities found in the dendritic trees, but the resulting pictures (Figure 3 in the paper) are striking. They provide a real sense of the high density of channels in the AIS and Ranvier nodes.

[Hu et al., 2009]

This paper titled "*Distinct contributions of $Na_v1.6$ and $Na_v1.2$ in action potential initiation and backpropagation*" explored the role of two distinct sodium channels subtype and their respective contributions to the initiation of an AP. The experimental part of this study observed the expression of $Na_v1.6$ and $Na_v1.2$ on stained slices on rat prefrontal cortex and measured the Na^+ currents at different positions. They identified the density of the two sodium channel types. They showed that the sodium channels with the highest activation threshold (1.2, whose voltage threshold for opening is about 10 mV higher than for 1.6) were preferentially located in the proximal part of the AIS, i.e. the part closest to the cell body or "soma" which collects currents from the dendrites and feeds them to the AIS. These 1.2 channels were almost absent in the distal part which connects up to the axon. The other sodium channel type (1.6), with the lower activation threshold, had a complementary distribution, with his highest density at the distal AIS.

2.2 Previous numerical studies

Before attempting to combine the two concepts of AP initiation and CLS of sodiums channels kinetics into one model, we need to look closely at the existing numerical models from each concept separately. We need to make sure our model can reproduce, qualitatively at least, the relevant behaviours found previously, and insure that model components borrowed from these studies are compatible.

2.2.1 On the initiation at the AIS

There are numerous models of action potential generation in a single cell and along an axon, following the original work of Hodgkin and Huxley (HH). But work that specifically includes the AIS has been rarer to find. We searched for models that had simple channel dynamics, preferably like the standard HH model, and that had a spatial description of the axon. Three numerical studies of AP initiation stood out.

[Mainen et al., 1995]

In a attempt to settle the issue of the existence of dendritic spikes *Mainen et al.* simulated a full rat layer 5 pyramidal cell in their paper "*A model of spike initiation in neocortical pyramidal neurons*". As far as we know, this is the first computational model pointing clearly to the AIS as the site of action potential initiation. They also described the phenomenon of back-propagation of action potentials generated at the soma into the dendritic tree as the source of spikes detected in previous experimental studies. The model they used is very similar to ours with the exception of the dendritic tree, which we chose to replace with a single passive compartment. Most parameters are similar and based on the original Hodgkin-Huxley Model.

[Hu et al., 2009]

We already mentioned this article for its experimental part. However, the study also has a numerical part to explore the role of each channel subtype identified in their paper. They modelled a complete neuron using the software NEURON 6. They used a previously developed multi-compartmental model of a layer 5 cortical pyramidal cell, to which they added a 50 μm long AIS of uniform diameter between the soma and the rest of the axon. They found using this simulated axon that each channel had distinct functions in the initiation of the action potential: $Na_v1.6$ channels were mostly responsible for the initiation due to their low threshold of activation, while the $Na_v1.2$ channels were responsible for the backpropagation. Our own model below was inspired by their model, which also motivated us to investigate the contribution of the effect of the spatial distribution of the damaged channels on the AIS.

[Brette, 2013]

This paper titled "*Sharpness of Spike Initiation in Neurons Explained by Compartmentalization*" solves an inconsistency between the standard HH single-compartment theory and most electrophysiological measurements. Patch clamp measurements of the sodium channel kinetics have always shown values of the Boltzmann slope factor for activation around 5 - 10 mV (see [Angelino and Brenner, 2007] for an exhaustive list of Na_v channel properties).

However, simulations in a single compartment model with those values are not compatible with the rapid onset of spikes usually recorded on cortical neurons. The author suggests a simple two-compartment model, a passive soma connected to an active AIS. This new model is sufficient to explain the sharpness of action potential initiation. This study showed both that single-compartment modelling is inadequate to describe some neurons and spatial localization of channels has an important effect on initiation.

2.2.2 On the coupled left-shift of Na_v channels

[Boucher et al., 2012]

This paper titled "Coupled left-shift of Nav channels: modelling the Na^+-loading and dysfunctional excitability of damaged axons" looks at the effects of trauma of the Na_V channels on the firing patterns of nodes of Ranvier. By varying the proportion of affected channels as well as the amount of coupled-left-shift (i.e. damage) for those affected channels, they explore many types of dysfunctional single neuron activity, such as bursting or transient firing. They included ionic pumps in their model, which are required to maintain constant concentrations of the key ions involved in action potential generation (sodium and potassium) both intra- and extracellularly. However, the increased rate of action potential generation in these damaged cells, related to the increase leakiness of sodium channels, leads to significant changes in the ionic concentrations that the pumps can not perfectly counteract. Their model thus allows the ion concentrations to vary with time as a function of the rate of generation of action potentials. This allowed them to study behaviours on larger time scales, namely transitions between apparently normal activity and abnormal activity once the concentration gradients had been sufficiently depleted.

In the next chapter we discuss the anatomical and physiological properties of the axon that are most relevant to analyzing the effect of AIS sodium channel composition on action potential initiation and propagation, both in health and as a function of coupled-left-shift.

Chapter 3

Anatomy and Physiology of the neuron

This thesis studies a specific behaviour in a specific part of a specialised cell through a simplified mathematical model. Before explaining the construction of this model in the next chapter, it is important to understand what is the object to model. Biological systems are notoriously complex and the brain epitomizes this complexity. The brain is an organ almost entirely made of nervous tissues that have an elaborate structure on multiple length scales. The two principal types of cells of the brain are the neuron and the glial cell. The former has had a lot more attention from neurophysiologist than the other and will also be the focus of the thesis. Even if the glial cells have an unavoidable effect on neurons, we concentrate on time and spatial scales where they have a negligible influence on the neuron.

In this chapter, we first go through the anatomy of the neuron, by describing it first as a general eukaryotic cell and then describing the specializations that make it a neuron. The second section will investigate the axon more specifically and how it's geometry and molecular organization shape its function. Finally, we have a look at pathologies associated with the axon initial segment.

3.1 Anatomy of the neuron

3.1.1 Historical context

We know today that the axon is part of the neuron, one of many types of cell, but this hasn't always been obvious. The mid-19th century saw the development of the cell theory: the idea that all living tissues are composed of individual cells arising from pre-existing cells and that the cell is the most basic unit of life. This theory was quickly and widely accepted as it was the culmination of two centuries of observations. Nevertheless, at the time there was not enough evidence to show that the nervous system was not an exception. The microscopical techniques then could not tell how the nerve cells and the nerve fibres were connected and whether the latter was a non-cellular basic unit or not. It took half a century, and many experimental innovations to finally come up with the neuron doctrine, establishing the neuron as a cell and describing its principal properties. (more in [Shepherd, 2015]) This illustrates how the nervous system has been exceptionally difficult to study compared to other organs and tissues. One of the controversial points in this historical example was the physical connection between what are now called the soma and the axon, the axon initial segment which is related to the subject of this thesis.

3.1.2 General cell anatomy

The neuron has all the basics components of a cell. It has all the necessary molecular machinery to survive. However, we are mostly interested in a few of those components: the extracellular and intracellular fluids, the membrane, and the ion-conducting transmembrane proteins (the ion channels). Other transmembrane proteins, as well as the nucleus, the cytoskeleton, and the mitochondria are also important to understand the context of the axonal injuries modeled in this thesis despite not being explicitely included in the numerical models. The following description of the components may not follow a usual order of presentation for the cell, as we ultimately want to present what is essential to our model.

The cell membrane

The cell membrane is what contains the cell. It is made of a lipid bilayer and embedded proteins. THere are three major classes of membrane lipids, phospholipids, glycolipids, and cholesterol. The bilayer is two parallel sheets of self-assembled lipids such that the hydrophobic lipid tails are isolated from the fluids on each side. The membrane itself acts as a two-dimensional fluid. The bilayer is permeable to nonpolar molecules, like oxygen and carbon dioxide and is very impermeable to ionic and polar molecules, like water and dissolved ions. This selective permeability allows the isolation of the cytosol, a property with many biochemical advantages. More specifically, in the case of charged molecules, it allows significant charge separation, effectively making the membrane an electric capacitance storing energy through chemical gradient and the electric field(more later in section 4.1.3. The thickness of the membrane is on the order of a few nanometers.

The extracellular and intracellular fluids

The extracellular and intracellular fluids are the complex aqueous solutions on each side of the membrane. Their ionic content being significant, these fluids are electrolytes. The intracellular fluid, also called the cytosol, has its composition regulated by the various membranes around and inside the cell. The extracellular fluid has a different composition and is regulated by all the surrounding cells. The maintenance of these fluids is crucial for the survival of the cell and all its functions.

In the case of one ion species, its concentration in each fluid will influence the kinetics of the reaction in which it is involved, but the ratio and the difference of concentration on each side will also have significant influence, respectively, the chemical potential difference and, for a charged solute, the voltage difference. Many important biochemical and biophysical mechanism, such as the action potential, rely on these transmembrane variables.

The volume of these fluids varies with each cell. In an axon, the volume of the intracellular fluids is the entire space contained by the cylindrical cellular membrane. In other parts of the neuron, fluids included in other large organelles such as the endoplasmic reticulum is not included in the intracellular fluid. The extracellular fluid is bounded by the cellular

membrane of the neurons and of the surrounding cells.

The transmembrane transport proteins

The transmembrane transport proteins span the entire thickness of the membrane and move molecules across it. They make the membrane interact with the fluids on each side by taking advantage of the chemical and electrical potential gradients described above. The cell membrane is crowded with many more types of proteins but they are omitted from this simplified description of a cell.

The simplest type of transport protein is a channel. It allows molecules to passively diffuse across the membrane through a pore. A channel can be selective, ie. only allowing specific molecules. It can also be gated, ie. requiring specific conditions to be permeable. The gating can be influenced by the voltage difference across the membrane or the binding to a specific molecule. They are called voltage-gated and ligand-gated channels respectively. Channels are categorized according to their principal permeant molecules and their gating mechanism. For example the channels included in our model are the sodium voltage-gated channels and the potassium voltage-gated channels, all examples of ion channels. Another example would be the calcium-activated potassium channel. A family of channels can include many channels with different properties and can be identified with their electric behaviour, their chemical kinetics, the genes encoding them or any context-dependent unique properties. We talk about specific voltage-gated channels in the next section.

Carrier proteins are another type of transport protein. Instead of letting the molecules diffuse, they bind to them on one side of the membrane and unbind from them on the other side. They can move one or multiple molecules and they can either move the molecules with or against their concentration gradient. In the latter case, they require additional energy through ATP hydrolysis and are called active transporters. The active transporters are the only proteins that can increase the energy stored across the membrane and therefore are essential in maintaining all the concentration gradients. The sodium-potassium pump, Na/K ATPase, is the active transporter maintaining the most important gradients for the neuron, low inner Na and high inner K.

Cotransporters are carrier proteins that carry different molecules at once, transferring

the energy between different concentration gradients. They allow for the fine-tuning of each concentration gradient. For example, the sodium-calcium exchanger is a costransporter using the energy in sodium gradient to remove the calcium from the cytosol where it is toxic.

The carrier proteins are described here as they are part of what establishes the reversal potentials used in our model. Their effects are also included in some of the models that inspired ours. However, we chose to not explicitly include them in our model because they add too much complexity for the small effects they have at the time scale of our simulation. Nevertheless, they should not be overlooked too quickly if someone chooses to expand on our model.

The cytoskeleton

The cytoskeleton is the structural support of the cell. It interacts closely with the membrane to give it its shape and regulate its activities by binding to many of its proteins. Parts of the cytoskeleton also act as the 'rails' in trafficking organelles along the axon. The disruption of this interaction has important repercussions. The extracellular matrix is the external and less critical equivalent of the cytoskeleton but still has an important effect on neuron activities [Verkman, 2013].

The mitochondria

The mitochondria are the source of the ATP used throughout the cell, including the the Na/K ATPase briefly discussed above. They stored the energy from cellular respiration by phosphorylating ADP into ATP. They are located in every part of the neuron, even the thinnest parts of the axon. [Berthold et al., 1993]. They are organized in long filaments in the cytoplasm. [Skulachev, 2001]. At the source of all the energy used, their proper functioning is crucial. Not only does a lack of nutrient (ischemic attack) can endanger the neuron, many other neuropathies can be directly linked to the mitochondria [Baloh, 2008].

The nucleus

The nucleus contains the gene of the cell required to build all the proteins with the help of other organelles, like the rough endoplasmic reticulum and the ribosomes. They are involved

in the maintenance of the overall health of the cell by manufacturing its building blocks and therefore are particularly important in a reaction to an injury.

3.1.3 Voltage-gated ion channels

The previous section was a simplified description of some cell components for any animal cell. The differences between the anatomy of a neuron and of any other cell are diverse but only a few are needed to explain one key function of the neuron: the conduction and initiation of an action potential. A cell has to be electrically excitable to produce an action potential. This means that some ion channels need to have a non-linear response to an electrical stimulus. The sodium voltage-gated channels and the potassium voltage-gated channels are responsible for the greatest current across the membrane of a typical neuron during an action potential and all exhibit this non-linear response by having multiple conformational states as it will be explained in section 4.1.2 .

The voltage-gated sodium channels

The voltage-gated sodium channels (Na_v channels) are a family of channels present on all neurons as well as other cells (eg. heart). As the name says, they are mostly permeable to sodium ions and the voltage modulates their conductances across the membrane. The existence of these channels were hypothesized since the detection of the sodium current in squid axon [Hodgkin and Huxley, 1952b]. However, the actual proteins making up these channels were not identified until the 1980s (see review [Catterall, 2000]). Even if their tridimensional structure has only been studied in detail recently [Payandeh et al., 2011], their well-known amino acid sequence has given a good understanding of its structure. A Na_v channel is made up of an α subunit and one or more β subunit. The α subunit is made of six tubular-shaped transmembrane segments in each of the four homologous domains. One of the six segments is charged and acts as a voltage sensor. The four domains assemble together to form a pore, through which the sodium ions pass. The domains are connected by intracellular loops, one of which can obstruct the opening of the pore and is responsible for the inactivation. The β subunits only have a single transmembrane segment and most of

their mass is in the extracellular fluid.

In mammals, there are nine different α subunits and they are remarkably similar: $Na_v1.x$ where x is between 1 and 9 [Yu and Catterall, 2003]. Five of them are found in neurons ($Na_v1.1$,$Na_v1.2$,$Na_v1.3$,$Na_v1.6$,$Na_v1.7$), one in skeletal muscle($Na_v1.4$), one in cardiac muscles ($Na_v1.5$) and the the rest dorsal root ganglion($Na_v1.8$,$Na_v1.9$). Many of these subtypes are expressed in combination on the same membrane [Hu et al., 2009] [Choi and Waxman, 2011] The subunits $Na_v1.2$ and $Na_v1.6$ are abundent in cortical neurons [Lorincz and Nusser, 2010] and are found to be essential in action potential initiation [Royeck et al., 2008] [Rush et al., 2005]. Na_v channels also have phosphorylations site that can affect their dynamics and is central to their plasticity [Cantrell and Catterall, 2001].

The voltage-gated potassium channel

The voltage-gated potassium channels (K_v channels) are another family of channels on the neuron. They are mostly permeable a to potassium ions. As the Na_v channels, it existence was hypothesized in the first studies of the different currents involved in nerve excitability.

The selective permeability of this channel was perplexing for a long time as the radius of potassium ion is smaller than for the sodium ion. The discovery of the selection mechanism [Doyle et al., 1998] was the object of a Nobel prize. The selection of the potassium ion is made with special binding sites in the pore that replaces the hydration shell of the ion. This interaction happens to be more favourable for the potassium ions.

The K_v is made of four similar α subunits, compared with the Na_v channels that domains on *one* subunit. The K_v channel is said to have tetrameric structure. One powerful feature of this structure is the ability to combine different types of α subunits [Isacoff et al., 1990] [Ruppersberg et al., 1990] , making the K_v a very diverse family of channels, especially compared to the sodium channels. The channel can also include β subunits to modulate its activties [Li et al., 2006]

3.1.4 The axon cytoskeleton

The cytoskeleton of the axon is very complex and is made of multiple interacting parts. They are essential in providing structural support and spatial organization for the various membrane proteins involved in the neuron's functions.

Actin filaments

Actin filaments are an important part of the cytoskeleton. Strong and highly flexible, they are polymers formed across the neuron and can be found close to the membrane. They are also responsible for the motility and reorganization of the dendrites and therefore as an important role in plasticity. [Susuki and Rasband, 2008]

Spectrin

Spectrin is another type of cytoskeleton protein having a scaffolding role for the membrane. Spectrins are attached to the actin filaments [Ogawa and Rasband, 2008]. The type βIV spectrin can be disrupted by calpain [Büki et al., 2000] causing the blebbing of the membrane. The type βIV is a specialized spectrin for the nodes and the AIS [Berghs et al., 2000].

AnkyrinG

The AnkyrinG is a scaffold protein connecting the Na_v channel, some K_v channel and the neurofascin to the spectrin connected to the membrane and the rest of the cytoskeleton. This protein is involved in the clustering of the channel and its immunostaining (ie. making it glow under a microscope) helps to identify the location of the sodium channels.

Neurofascin

Neurofascin is a cell adhsion molecule(CAM) connecting the interior cytoskeleton to the extracellular matrix. It plays an important role in the formation and the maintenance of specialized domains in the AIS and the nodes [Zonta et al., 2011] and their surrounding extracellular domain [Hedstrom et al., 2007].

3.2 Geometry and Protein distributions

3.2.1 General neuron geometry

The neuron has one of the most recognizable shapes of all the cells: a squiggly star with long fine tubes stemming from the vertices and branching like little trees. One of the tubes is longer and slightly thicker, and is sometime covered in long and regularly spaced beads. This simplified depiction describes the three main divisions of the geometry of the neuron: the star is the soma, the thicker tube is the axon and the trees are the dendrites and the axon terminals.

The dendrites are an arborescence of cellular projection reaching the surrounding neurons and axon terminal to receive the input from other neurons. They are a very complex part of the axon, their complex geometry and chemical properties makes them a very interesting subject of research.

The soma of the neuron is the thicker part of a neuron as it contains the nucleus and the rough reticulum endoplasmic, the protein factory of the cell, that supplies the entire length of the axon. In most cases its surrounding membrane receives the combined signal of the dendrites.

The axon is a very long process from the soma, usually unbranched and sometimes covered in myelin, a glial cell membrane wrapped multiple times around the axon. The axon takes the summed signal from the soma, initiates an action potential in its initial segment and propagate it to its terminal away from the soma. When myelenated, exposed segments, called nodes of Ranvier, placed at regular intervals, relay the action potentials.

The axon initial segment sits between the axon hillock of the soma and the rest of the axon. It has length in the tens of micrometers and has a slight taper, with its radius slightly larger proximally.

3.2.2 Ion channel localization

The polarity of the neuron, i.e. the direction in which the signal travels, is dictated by the localization of the voltage-gated ion channels. The specialization of the axon from all the

other extension happens at an early stage of the neuron growth [Barnes and Polleux, 2009]. Soon after, a segment of the axon close to the soma acquires specific features that will lead to a different channel densities than the rest of the axon. During development, the channels are maintained in place after their delivery by a diffusing barrier [Nakada et al., 2003]. This creates in the AIS very well delimited subdomains with different concentrations.

The $Na_v1.6$ and $Na_v1.2$ are the main ion channels of the axon [Martínez-Hernández et al., 2013] while the $Na_v1.1$ and $Na_v1.3$ are in the dendrites [Lorincz and Nusser, 2010] [Vacher et al., 2008] . In the axon, $Na_v1.6$ are heavily concentrated in the nodes and the distal part of the axon [Hu et al., 2009]. $Na_v1.2$ are expressed in the proximal AIS and the axon terminal.

The K_v channels are very diverse in the neuron. In the axon, the biggest potassium currents are created by the $K_v1.2$ channels. They are located at the distal part of the axon [Van Wart et al., 2007] and in the paranodes [Lai and Jan, 2006]. Other potassium channels are found in the nodes ($K_v3.x$ and $K_v7.x$) and the AIS $K_v3.x$.

The axon is molecularly more complex than what we could ever present here. A complete review of its physiology can be found here: [Debanne et al., 2011].

3.2.3 Action potential initiation in the axon initial segment

The AIS is a very specialized part of the neuron. Much energy is spent early on by the cell to ensure that it has a very specific channel distribution. Also a lot of energy must be spent to keep homeostasis on such a large conducting surface. This importance is justified by the fact that the action potential initiates at the AIS [Palmer and Stuart, 2006]. Although it has been hypothesized very early in the history of action potential recordings, it is only recently that the precision of the recording tools has been able to confirm that the AIS is indeed the site of initiation [Clark et al., 2009].

The AIS has a very large density of sodium channels, which is very important in the initiation phase of the action potential [Kole et al., 2008], as we will show in section 4.3. The presence of two distinct sodium channels subtype $Na_v1.6$ distally and $Na_v1.2$ proximally, plays a role in initiating an antidromic action potential back into the dendrites [Hu et al., 2009]. Its large density of potassium channels also plays an important role in regulating the shape of the action potential [Kole et al., 2007].

The excitability of the AIS is also very dependent on its geometry, as we will discuss in section 4.4. The AIS also has the ability to adapt and change its length and channel density [Grubb et al., 2011] [Kuba, 2010] [Kuba et al., 2010].

3.3 Pathology of the axon

With the AIS at the center of the action potential initiation, the nervous system is really affected anytime something goes wrong. Unique to the AIS in the axon is its plasticity, which is a double-edged sword as it can help the axon adapt to changes in excitability as well as having the plasticity mechanism to turn against it and destroy it [Schafer et al., 2009].

There are many disease with their origin at the AIS [Buffington and Rasband, 2011], some of which are channel related [Iwata, 2004]. They even found a relation between schizophrenia and aberrant axoaxonic synapses (synapses at the AIS) activity [Lewis et al., 2005], and a relation between bipolar disorder and abnormal AnkyrinG, very abundant at the AIS[Ferreira et al., 2008]. Closer to our subject of study, there are some specific types of injury we are interested in as they relate to parameters in our model.

3.3.1 Ischemic injury

Ischemic injury is basically the cells suffocating and drowning. When a cell and its mitochondria are deprived of oxygen, through limited blood flow, the production of ATP stops. A cell actively maintains the chemical gradients across its membrane, and these start to diffuse to equilibrium in absence of pumping. The cytoplasm is flooded with unwanted and toxic ions. More specifically calcium ions, held at very low concentration in normal situation and used for signaling, activate many chemical reactions to abnormal levels and can trigger apoptosis, cell death. A good analogy at the macroscopic level is the pulmonary edema where failure in proper pumping of the blood makes the lung filled with water, effectively drowning the person. One chemical process activated by calcium is the cleavage of the spectrin and ankyrin based cytoskeleton by calpain [Schafer et al., 2009]. As we described above, this part of the cytoskeleton is crucial in maintaining polarity in the AIS and connecting the axon to the extracellular matrix [Rasband, 2010].

3.3.2 Diffuse axonal injury

Diffuse axonal injury is a very common type of damage to the brain created by shearing forces applied to the white matter, made of myelinated axons. The damage can be seen at a macroscopic level because the brain undergoes rapid deformations. At the cellular level, the axon cytoskeleton is mechanically disrupted. The membrane can detach itself and bleb outward. The cell adhesion molecules are also disrupted and can detach from the extracellular matrix. Diffuse axonal injury is also characterized by an influx of Ca^{+}, leading to chemical cytoskeleton disruption. In mild diffuse axonal injury, like concussion, the brain has the ability to adapt with minimal long-term cognitive consequences [Baalman et al., 2013].

3.3.3 Coupled Left-shift in sodium channels

Diffuse axonal injury doesn't disrupt ion homeostasis as brutally as an ischemic injury. However, there's still an abnormal calcium concentration and cleavage of sensitive parts of the cytoskeleton. It was found that blocking sodium conductances protected the axon from this damage, identifying the sodium channel as the culprit [Wang et al., 2008]. We described these finding, an abnormal increase in sodium current, in the previous chapter. This increase in sodium current is an additional stress to the pumps and exchangers as they try to keep the homeostasis in check, allowing more calcium than usual inside the cell. The increased sodium also has deep effects on the functionality of the neuron, changing its firing pattern dramatically [Boucher et al., 2012] [Yu et al., 2012]. As we mention earlier, this model motivated our investigation of damage on the axon initial segment. For the rest of this thesis, the terms coupled left-shift (CLS) of the sodium channels and damaged sodium channel will be used interchangeably.

Chapter 4

Theory of Action Potential Initiation and Propagation

In this chapter we develop the theory of the action potential in an axon. We start by describing the biophysics of the components presented in the previous chapter (4.1). Then we describe how these components combine to reproduce the nonlinear behaviour of the current across the membrane (4.2). This will allow us to describe the action potential, in particular how and when it initiates (4.3). Finally, we will talk about the propagation by presenting the cable equation and how it applies to the axon and its different segments (4.4). The equations 4.18 and 4.34 derived in here will be used in the following chapters.

4.1 Biological elements of the axon as electronic elements

The action potential is an electrical phenomena involving the movement of charged particles around the axon. It makes sense to model the membrane of the axon as a circuit. We thus summarize many past efforts to formulate an electric equivalent of the main axon component involved in the initiation and propagation of the axon initial segment: the membrane itself, the surrounding electrolytes, and the ion channels.

4.1.1 Electrolytes as conductors

Electrolytes are charged particles that behave as solutes in a solvent. These charged particles are present in quantities such that the total charge is kept neutral overall even if it can be locally non-zero.

Each charged particle is affected by forces of two types: the first is from the surrounding particles constantly bumping into it and the second is from an external applied electrical field, if present. The forces created by the surrounding particles manifest themselves in two ways: a drag force and variation of free energy G. The drag always opposes any force applied to the particles, such that the acceleration dies very fast and the speed becomes proportional to the force almost instantaneously. The addition of particles in a region causes an increase in the free energy of this region, since it increases the interactions ('bumpings') between the particles. The collective motion of the particles is such that they will always try to move in a way that minimizes the free energy. Finally, the electrical field acts as an external force and contributes to the free energy. The resulting movement of ions is described by the current $\vec{J}_a$ in the Nernst-Planck equation:

$$\begin{aligned}
\vec{J}_a &= -\beta D_a \nabla G_a \\
&= -\beta D_a \left(c_a \nabla \mu_a - e z_a c_a \nabla V\right) \\
&= -\beta D_a \left(c_a \nabla (\beta^{-1} \ln c_a) - e z_a c_a \nabla V\right) \\
&= -D_a \left(\nabla c_a - z_a c_a \frac{\nabla V}{V_T}\right)
\end{aligned} \tag{4.1}$$

where β is the thermodynamic beta $1/kT$, e the elementary charge, $V_T \equiv 1/e\beta \approx 23\text{mV}$ is the thermal voltage, V is the electric potential, D_a in the diffusion constant of particle a, G_a is its free energy, c_a its concentration, μ_a its chemical potential and z_a its valence.

We consider the electrolytes to be uniformly distributed on each side of the membrane, so that the spatial gradients are zero. Combining all the electrolytes with a simplified equation

4.1 gives us the electric current density $\vec{J_e}$:

$$\begin{aligned}\vec{J_e} &= \sum_a z_a \vec{J_a} = \sum z_a^2 c_a D_a \frac{\nabla V}{V_T} \\ \nabla V &= \frac{V_T}{\sum_a z_a^2 c_a D_a} \vec{J_e} \\ \nabla V &= \rho \vec{J_e} \end{aligned} \tag{4.2}$$

where ρ is the resistivity of the electrolytes present in the current. Equation 4.2 is simply Ohm's law. Therefore, an electrolyte can be reduced to a simple linear resistance.

4.1.2 Channels as nonlinear conductors

The previous chapter described in length the channels, their composition and how they behave experimentally. We assumed intuitively that the channels conduct and react in complex ways to an electric field. Here we formalize this understanding first by presenting the conducting part and then by explaining how the gating can be modelled.

Conduction

As electrolytes, channels also transport ions. However, they usually let only one type ion through, excluding even water molecules, as though the channels themselves act as a solvent. Nernst-Planck equation still describes quite well the movement of ions through channels; however, now the concentration gradient does change from one side to the other. As we are only interested in what is happening along one axis, the one through the pore formed by the channel, we only use one component of equation 4.1. We also assume V to vary linearly over the distance L of the pore:

$$J_a = -D_a \left(\frac{dc_a}{dr} - z_a c_a \frac{\Delta V}{VL} \right)$$

By separation of variables (dr on one side of the equation, the rest on the other side) we get the Goldman-Hodgkin-Katz(GHK) flux equation:

$$J_{a,e} = ez_a^2 \frac{D_a}{L} \frac{\Delta V}{V_T} \frac{c_{a,\text{in}} - c_{a,\text{out}} e^{-z_a \frac{\Delta V}{V_T}}}{1 - e^{-z_a \frac{\Delta V}{V_T}}} \tag{4.3}$$

$$\approx g_a \left(\Delta V - E_a\right)) \ . \tag{4.4}$$

where g_a is an approximation of the slope of equation 4.3 in the relevant range, usually about the resting potential.

The equation 4.3 is useful when $c_{a,\text{in}}$ and $c_{a,\text{out}}$ are sufficiently different, as in the case of calcium ions where concentrations are of different orders of magnitude on each side of the membrane. The conductance is then rectified.

The equation 4.4 is appropriate when the ion concentrations are of the same order of magnitude, which is mostly the case for sodium and potassium.

Gating

In the previous equations, we had g_a and D_a, the conductance and the diffusion coefficient respectively, representing the ease that an ion a has to pass through the pore formed by the channel. Each conformation of a channel has a particular g_a (and therefore D_a, but we will only consider the conductance from now on). A flexible and accurate way to model this would be to set the conductance as the combination of all the conformations of conductances weighted by their probability:

$$g_a = \sum_i p_i g_{a,i}$$

where $\sum_i p_i = 1$.

The conformation probabilities depends on external properties, particularly voltage, that change in time. We model the evolution over time of the p_i using a Markhov model:

$$\begin{bmatrix} p_1(t+dt) \\ \vdots \\ p_n(t+dt) \end{bmatrix} = \begin{bmatrix} \alpha_{11}(V,t) & \dots & \alpha_{1n}(V,t) \\ \vdots & \ddots & \vdots \\ \alpha_{n1}(V,t) & \dots & \alpha_{nn}(V,t) \end{bmatrix} \begin{bmatrix} p_1(t) \\ \vdots \\ p_n(t) \end{bmatrix}$$

This model in its general form would be very long to compute and would increase the complexity of the system to unmanageable scales, especially because this level of detail would also require the accounting for all small variants of one channel.

To make a simple model of the gating, we have to make a few assumptions. First, we only consider one state to be conducting:

$$g_a = \bar{g}_a p_0 \,.$$

Second, we assume the space of states to consist of simple products of independent state spaces, some present q_j times, with all having only one conducting state:

$$p_0 = \prod_j p_j^{q_j} \,.$$

The p_j are called gating variables, and they all evolve independently:

$$\begin{bmatrix} p_j(t+dt) \\ 1-p_j(t+dt) \end{bmatrix} = \begin{bmatrix} 1-\alpha_j(V)dt & \alpha_j(V)dt \\ \beta_j(V)dt & 1-\beta_j(V)dt \end{bmatrix} \begin{bmatrix} p_j(t) \\ 1-p_j(t) \end{bmatrix}$$

which simplifies to:

$$\dot{p}_j = \alpha_{p_j}(V)(1-p_j) - \beta_{p_j}(V)p_j \tag{4.5}$$

$$= \tau_{p_j}^{-1}(V)\left(p_j^{\infty}(V) - p\right) \tag{4.6}$$

where

$$\tau_{p_j}(V) \equiv \frac{1}{\alpha_{p_j}(V) + \beta_{p_j}(V)} \tag{4.7}$$

$$p_j^{\infty}(V) \equiv \frac{\alpha(V)}{\alpha_{p_j} + \beta_{p_j}} \,. \tag{4.8}$$

The parameters α and β can be obtained from fits to experimental data. Gates are added and their multiplicities chosen to better fit the data. It may or may not reflect the actual gating mechanism, but provides a simpler yet accurate model to simulate and analyze.

4.1.3 Membrane

The membrane separates the extracellular and intracellular volumes, keeping their ionic content from diffusing into each other. The membrane can keep this separation small, making a powerful chemical and electric gradient readily accessible to the transmembrane proteins such as the ion channels. The chemical gradient is already accounted for in our model in equation 4.4 as E_a.

The electric gradient is created by an imbalance of charge across both sides of the membrane. Because the membrane is a very good insulator, the charges can't diffuse easily back to neutrality. Any leaking through the channels is quickly counteracted by various pumps and co-transporters. This charge separation is modeled as a capacitor where the inward currents are positive by convention:

$$\begin{aligned} CV &= Q \\ C\dot{V} &= -I\,. \end{aligned} \tag{4.9}$$

4.2 Conduction across the membrane and the action potential

In the previous chapter we presented multiple parts of the axon and their chemical and electrical properties. In this section we look at how they interact with each other on a small patch of membrane and present a simplified model that will be used for the rest of this thesis.

4.2.1 The membrane as a nonlinear RC circuit

In summary, we have the ions of the electrolytes as charge carriers, the ionic concentration gradients as voltage sources, the membrane as a capacitor and the channels as conductors. All channels selective for ion species A are connected in parallel, adding their conductance per surface area $g_{A,i}$ together. The resulting conductance is then in series with a voltage source E_A, corresponding to the reversal potential for ion species A. All the currents per unit area of membrane associated with these ion-specific parallel circuits add up with the capacitive current through the membrane capacitance per surface area c_m, as well as other external currents I_ext; the sum is zero due to conservation of charge.

An equation for the voltage across the membrane V_m arises:

$$C_\mathrm{m}\dot{V}_\mathrm{m} = -I_\mathrm{ext} - \sum_A \left(\left(\sum_i g_{A,i} \right) (V_\mathrm{m} - E_A) \right). \tag{4.10}$$

We recognize the equation for an RC circuit

$$\dot{V}_{\mathrm{m}} = -\tau_{\mathrm{m}} \left(V_{\mathrm{m}} - E_{\mathrm{m}}\right) \tag{4.11}$$

where the membrane time constant (τ_{m}) and the membrane reversal potential (E_{m}) are

$$\tau_{\mathrm{m}} \equiv \frac{g_{\mathrm{m}}}{c_{\mathrm{m}}} \tag{4.12}$$

$$E_{\mathrm{m}} \equiv \frac{\sum_A g_A E_A + I_{\mathrm{ext}}}{g_{\mathrm{m}}} \tag{4.13}$$

$$g_{\mathrm{m}} \equiv \sum_A g_A \tag{4.14}$$

$$g_A \equiv \sum_i g_{A,i} \,. \tag{4.15}$$

As expected, the equilibrium potential is the reversal potential. The time constant is also independent of the surface area which makes the equation (4.10) independent of geometry.

In general the conduction g_A can be any combination of channels permeable to A with diverse gating schemes as described in section 4.1.2:

$$g_{A,i} = \bar{g}_{A,i} \prod_j p_{A,i,j}^{q_{A,i,j}} \tag{4.16}$$

$$\dot{p}_{A,i,j} = -\tau_{A,i,j}(V) \left(p_{A,i,j} - p^{\infty}_{A,i,j}(V)\right) \,. \tag{4.17}$$

4.2.2 Hodgkin-Huxley model

In summary, every ion A has its reversal potential E_A and its channels $g_{A,i}$, and every channel has its gates $p_{A,i,j}$ with their own multiplier $q_{A,i,j}$. The complexity of this system grows fast with every added component. It is important to select with care what is included to make sure it captures the phenomena we are studying, all the while being simple enough to limit the number of parameters. We also strive to keep the model as biologically realistic as possible.

There are many minimal models that we could have used for our study. However, to relate to specific previous studies [Boucher et al., 2012] [Lachance et al., 2014] [Mainen et al., 1995] the classical Hodgkin-Huxley [Hodgkin and Huxley, 1952a] was chosen. It models three ion species: sodium, potassium and leak (ie. all the other ions). Each has one channel type:

the sodium channel has two gates, the potassium channel one and the leak channel (ie. everything else) none. We extend this model to include a coupled left-shift (CLS) by adding another channel for the sodium. It has a distinct gating variable but otherwise shares the same dynamics; however it has an offset to the voltage (V_{LS}) as an added parameter:

$$\begin{aligned} C_m\dot{V} = &- I_{\mathrm{inj}} - \left(\bar{g}_{\mathrm{Na}} m^3 h + \bar{g}_{\mathrm{Na,LS}} m_{\mathrm{LS}}^3 h_{\mathrm{LS}}\right)(V - E_{\mathrm{Na}}) \\ &- \bar{g}_{\mathrm{K}} n^4 (V - E_{\mathrm{K}}) - g_{\mathrm{L}} (V - E_{\mathrm{L}}) \end{aligned} \tag{4.18a}$$

$$\dot{m} = -\tau_m(V)^{-1}(m - m_\infty(V)) \tag{4.18b}$$

$$\dot{h} = -\tau_h(V)^{-1}(h - h_\infty(V)) \tag{4.18c}$$

$$\dot{n} = -\tau_n(V)^{-1}(n - n_\infty(V)) \tag{4.18d}$$

$$\dot{m}_{\mathrm{LS}} = \dot{m}(V + V_{\mathrm{LS}}) \tag{4.18e}$$

$$\dot{h}_{\mathrm{LS}} = \dot{h}(V + V_{\mathrm{LS}})\,. \tag{4.18f}$$

The parameters are given in table 4.1 and the equations for m_∞,h_∞,n_∞, τ_m, τ_m are given by equations 4.8 and 4.7 with the α and β for each gating variable given by:

$$\begin{aligned} \alpha_m(V) &= 0.1\frac{V+40}{1+\exp\left[-\frac{V+40}{10}\right]} \\ \beta_m(V) &= 4\exp\left[-\frac{V+65}{18}\right] \\ \alpha_h(V) &= 0.07\exp\left[-\frac{V+65}{20}\right] \\ \beta_h(V) &= \frac{1}{1+\exp\left[\frac{V+65}{20}\right]} \\ \alpha_n(V) &= 0.01\frac{V+55}{1-\exp\left[-\frac{V+55}{10}\right]} \\ \beta_n(V) &= 0.125\exp\left[-\frac{V+65}{80}\right]\,. \end{aligned}$$

The system in 4.18 will be used in the numerical simulations of the next chapter.

Table 4.1: Parameters of the Hodgkin-Huxley equations 4.18. γ is the proportion of sodium channels affected by CLS.

Variables		Value	Units
Membrane Capacitance	C_m	1.0	$[\mu\text{Fcm}^2]$
Normal sodium conductance	$\bar{g}_{\text{Na}}$	$120.0 \cdot (1-\gamma)$	$[\text{mScm}^2]$
CLS sodium conductance	$\bar{g}_{\text{Na,CLS}}$	$120.0 \cdot \gamma$	$[\text{mScm}^2]$
Potassium conductance	$\bar{g}_{\text{K}}$	36.0	$[\text{mScm}^2]$
Leak conductance	g_{L}	0.25	$[\text{mScm}^2]$
Sodium reversal potential	E_{Na}	51.5	[mV]
Potassium reversal potential	E_{K}	−81.3.0	[mV]
Leak reversal potential	E_{K}	−59.9	[mV]

4.2.3 Reduced model

Our model (equations 4.18) has six dimensions, which makes it very complex. Usually the variables m and m_{LS} are as fast as V and therefore we can simplify the system by replacing them in 5.1a by their steady state values $m_\infty(V)$ and $m_\infty(V + V_{\text{LS}})$, respectively:

$$C_m\dot{V} = -I_{\text{inj}} - \left(\bar{g}_{\text{Na}} m_\infty(V)^3 h + \bar{g}_{\text{Na,LS}} m_\infty(V+V_{\text{LS}})^3 h_{\text{LS}}\right)(V - E_{\text{Na}}) \tag{4.19a}$$

$$\dot{h} = -\tau_h(V)\,(h - h_\infty(V)) \tag{4.19b}$$

$$\dot{n} = -\tau_n(V)\,(n - n_\infty(V)) \tag{4.19c}$$

$$\dot{h}_{\text{LS}} = \dot{h}(V + V_{\text{LS}})\,. \tag{4.19d}$$

These equations are useful to better understand the dynamics of 4.18. A general intuition of the interaction of the many variables is given by plotting the fixed points of $\dot{(V)}$ in 4.19a with the solution of 4.18 as done in figures 4.1 and 4.2.

4.3 Action potential

One important solution to the equations 4.18 is the action potential created by varying I_{inj} or by choosing an appropriate initial V. Figure 4.1 shows such an action potential solution. We also show in figure 4.2 special cases of initiation that will be discussed in the following sections.

We added a graph of the gating variables to make their role in the action potential explicit. We added to the voltage graph the solutions of $\dot{V}(V) = 0$ with $\dot{V}$ as defined in equation 4.19a. Drawing those 'fixed points' will help understand the dynamics of the action potential in the following section where we explore its phases.

4.3.1 Phases of the action potential

The action potential can be divided into three phases.

1. The *rising phase* or *initiation phase* caused by the fast opening of the sodium channels. The increase in sodium conductivity is the result of a membrane voltage depolarization usually caused by positive charge injected in the intracellular volume.

2. The *falling phase* follows the peak of the previous rising phase. At this point the sodium channels starts to inactivate in response to the high voltage; and as the potassium channels activate, they will draw the membrane potential to the lower (more negative) potassium reversal potential. In figure 4.1, we see that the stable equilibrium in the positive voltage, the one to which the membrane potential was attracted to in the rising phase, eventually disappears by colliding with an unstable equilibrium point in the falling phase. This bifurcation in a reduced system enables the membrane potential to repolarize to the only stable equilibrium left close to the potassium reversal potential.

3. The *refractory phase* is the phase during which an action potential can not be initiated, as the sodium channels are still inactivated and as the potassium and leak conductances dominate. The refractory phase is further divided into an absolute refractory phase and a relative refractory phase. During the latter, an action potential can still be initiated if the cell receives a sufficiently large depolarizing input.

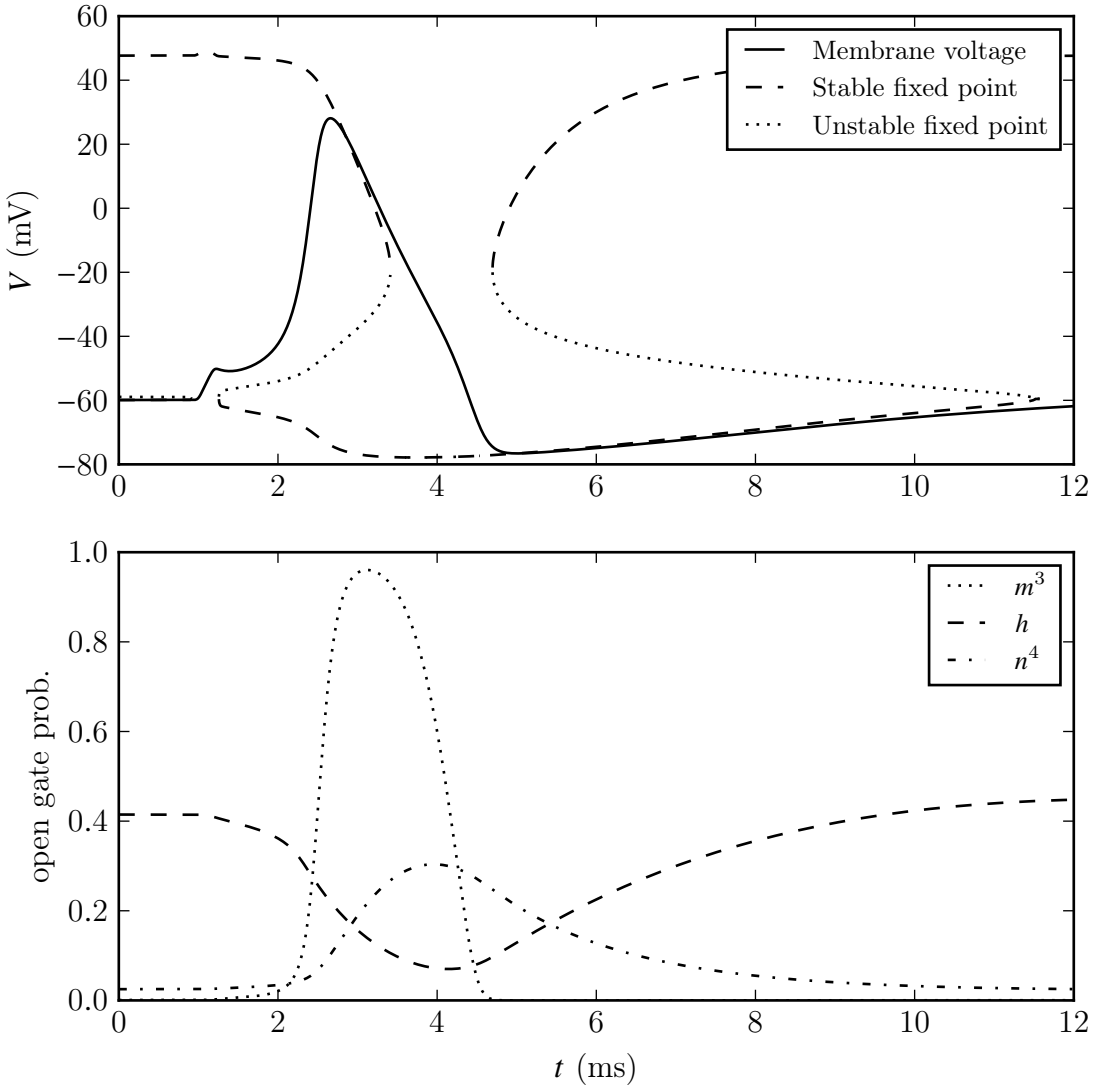

Figure 4.1: *An action potential. This is a solution of equations 4.18 with* $I = 59\mu\text{Acm}^{-2}$ *applied at* $t = 1\text{ms}$ *for* 0.2ms. *The corresponding stable and unstable fixed points of equation 4.19 are plotted with the membrane voltage using the values of* h *and* n *plotted in the bottom half.*

Those phases we just presented are subjective and not well delimited. They can be even defined differently or other phases can be added to help describe better the action potential. A phase called the afterhyperpolarization, which sits between the falling phase and the refractory phases as described below, is often added to the list as it describes how the membrane voltage undershoots the resting potential. We are particularly interested in the initiation phase. We want to find the criteria for a depolarizing stimulus that leads to this first phase.

4.3.2 Threshold

The threshold is difficult to define for a neuron. A strong injected current will initiate an action potential while a weak injected current will not. Therefore there must be a specific current above which an action potential initiates and below which it does not, i.e. a threshold current. But a current slightly higher than this threshold might initiate when applied suddenly, but wouldn't when the current is gradually ramped up to this same value. Defining the threshold as a charge, a voltage increase or a rate of voltage increase can not generally predict the initiation.

Experimentally, when the internal dynamics of the membrane are hidden, and only few observations are available such as the voltage or some selected ionic currents, finding the threshold becomes a very subjective process, requiring the skillful experiences of physiologists. A common definition for the threshold is a point at which the (first, second or even third) temporal derivatives reached some *ad hoc* value(s).

A comprehensive review of several methods of threshold detection [Sekerli et al., 2004] shows that many of them require some *a priori* choice of a good measurement parameter. This knowledge is not necessarily transferable between different types of neurons, due to the use of different measuring techniques and data sampling rate. Consequently, visual detection may in some cases still be as valid and objective as existing automated methods.

Numerically and theoretically, there's no limit on the knowledge of the system. It is possible to predict initiation using all the variables available, even in an analytically elegant way. In [Platkiewicz and Brette, 2010] we have an example of attempt to describe the threshold in term of its dynamics in a model based on the HH formalism. They considered

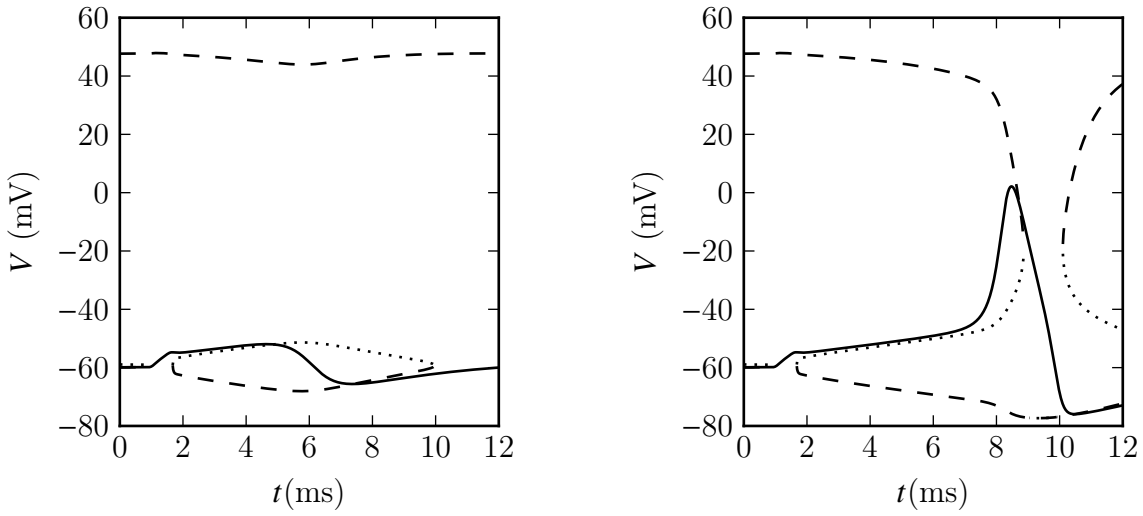

Figure 4.2: *Failure of action potential initiation and near-threshold initiation. (a) The figure on the left shows the solution to the HH equations 4.18 when the current is not sufficient to create an action potential. (b) The figure on the right shows an action potential with a current just above the threshold. We note the length of the initiation being around* 6ms*, a very extreme case by manually adjusting the injected current to 7 significant digits. We also note the peak of the action potential is very low at around* 0mV*. The dashed (dotted) lines denote the location of the stable (unstable) fixed point.*

a general equation,

$$\dot{V} = f(V) + \frac{1}{C}I$$

where $f(V)$ is the sum of all voltage-dependent currents. In our model, this would only be the sum of all the channel currents. I is all the external currents. The authors define two types of threshold using this equation. The first is the slow threshold $V = \theta_s$ such that $f'(\theta_s) = 0$, a saddle-node bifurcation of $\dot{V}$ for the parameter I. This threshold only works when I varies sufficiently slowly to let V go well above θ_s before the bifurcation is traversed in reverse to recreate the stable node at the resting potential. The second type is the fast threshold θ_q such that $f(\theta_q) = 0$ and $f(\theta_q) > 0$. This is the case where I returns quickly to zero and V simply has to be past the unstable fixed point of $f(V)$ to initiate the action potential.

4.3.3 Initiation Timing

Inspired by this formalism, we can try to find the delay required to generate an action potential once the threshold is crossed. We use the slow threshold definition to simplify the dynamics $f(V)$ around this point as a simple quadratic equation. We add a parameter ϕ_t^2 such that our quadratic curves best fit the points between θ_s and θ_q. We model this using an non-dimensional voltage ϕ for simplicity:

$$\dot{\phi} = a\left((\phi - \theta_s)^2 - \phi_t^2\right), \tag{4.20}$$

which has the solution :

$$\phi(t) = \theta_s + \phi_t \frac{\frac{\phi(0)-\theta_s}{\phi_t} - \tanh(a\phi_t t)}{1 - \frac{\phi(0)-\theta_s}{\phi_t}\tanh(a\phi_t t)}. \tag{4.21}$$

We see that for some values of $\phi(0)$, this solution diverges. This is the equivalent of an action potential in our simplified system. Solving for the zero of the denominator in 4.21, we have the time at which this divergence occurs:

$$t^* = -\frac{1}{a\phi_t} \ln\left(\frac{\phi(0) - \phi_{th}}{\phi(0) + \phi_{th}}\right) \tag{4.22}$$

where $\phi_{th} = \theta_s + \phi_t$.

In the following chapter we will use this result to fit the delay of action potential initiation following stimulus onset, versus stimulus strength data. This will yield a measured delay Δt of action potential initiation that follows an adapted version of the previous equation for t^*:

$$\Delta t = t_o + \tau_{\text{sens}} \ln\left(\frac{V_o - V_{\text{th}}}{V_o + V_{\text{th}}}\right) . \tag{4.23}$$

Note that, as these fits will be done using the full model, there is an additional fixed finite propagation time t_o that needs to be taken into account in addition to t^*. This parameter will be fitted along with the other ones in this expression, including the newly defined sensitivity parameter τ_{sens}, in the results surrounding figure 5.6.

4.4 Conduction along the axon

Up to now we only considered an infinitesimal patch of membrane. The axon is long enough that its membrane is usually not equipotential. This voltage gradient along the axon leads to axial currents able to excite adjacent segments of the membrane, which in turn excite other segments and so on. We will describe this process by deriving the cable equation. We will discuss the implication of geometry, particularly in the AIS and talk about the boundary conditions between the different segments of the axon.

4.4.1 Cable equation

Uniform axon

To greatly simplify our cable equation, we assume the current to be uniform radially and azimuthally. We divide the axon into infinitesimal slices perpendicular to the axis of the axon. We describe their geometry only by their cross-section area A and perimeter p.

To connect the patches of membrane together we introduce the continuity condition

$$\frac{d}{dz}I_z = -pJ_m(V) \tag{4.24}$$

where I_z is the axial current in A and J_m is the total membrane current density in $\frac{\mathrm{A}}{\mathrm{cm}^2}$, including the capacitance current. The axial current moves through the cytoplasm, which acts like an ohmic conductor as in the equation 4.2. We can rewrite in one dimension:

$$\frac{d}{dz}V = \frac{\rho_a}{A}I_z\,. \tag{4.25}$$

where ρ_a is the axoplasmic resistivity.

Putting 4.24 and 4.25 together, we get the cable equation

$$\frac{d^2}{dz^2}V - \frac{\rho_a p}{A}J_m(V) = 0\,. \tag{4.26}$$

When J_m is linear and the geometry is that of a perfectly uniform cylinder ($p = 2\pi r$ and $A = \pi r^2$) we obtain the well-known linear cable equation:

$$\begin{aligned}\frac{d^2}{dz^2}V - \frac{2\rho_a}{r}\left(C_m\frac{d}{dt}V + g(V - V_o) + I(x,t)\right) &= 0\\ \lambda^2\frac{d^2}{dz^2}V - \tau\frac{d}{dt}V - (V - V_o) &= g^{-1}I\end{aligned} \tag{4.27}$$

where $\lambda \equiv \sqrt{\frac{r}{2\rho_a g}}$ and $\tau \equiv \frac{C_m}{g}$ are the length constant and the time constant, respectively. The solution of 4.27 is

$$V(x,t) = V_o + \frac{1}{\sqrt{2\tau t}\lambda}\left(\tau(V(x,t=0) - V_o) - \frac{1}{g}I(x,t)\right) * e^{-\frac{t}{\tau}}e^{-\frac{\left(\frac{x}{\lambda}\right)^2}{4\left(\frac{t}{\tau}\right)}} \tag{4.28}$$

which is simply diffusive behaviour.

Diffusion alone doesn't give a propagating solution; the only way an axon such as we described so far can faithfully propagate a signal is by having nonlinearity in the conduction, comparable to a reaction-diffusion process. Therefore, any propagation properties, such as velocity, are very dependent on the nonlinearity of J_m. For example, even if τ is really low, a slow activation of the sodium channels in the initiation phase will make the propagation very slow as well.

4.4.2 Threshold for propagation

Activating a long axon takes more current than a shorter one, because of the increased area. We are not interested in uniform current injection, but a very localized injection still requires a stronger current to generate an action potential and make it propagate. Let's take the case of an infinite cable at the resting potential. We want to find the minimal voltage at the injection point such that the action potential propagates, i.e. I_z points away from the injection site. By multiplying equations 4.24 and 4.25 again and integrating:

$$\int_{+\infty}^{0} I_z \frac{d}{dz} I_z \, dz = \frac{2\pi^2 r^3}{\rho_a} \int_{+\infty}^{0} J_m(V(z)) \frac{d}{dz} V \, dz$$
$$I_z(V)^2 = \frac{4\pi^2 r^3}{\rho_a} \int_{V_o}^{V} J(V) \, dV \, . \tag{4.29}$$

We want to find a V_{pth}, a propagation threshold, such that $I_z(V_{\text{pth}}) > 0$.

$$0 < \sqrt{\int_{V_o}^{V_{\text{pth}}} J_m(V) \, dV}$$
$$0 < \sqrt{\int_{V_o}^{V_{\text{uth}}} J_m(V) \, dV + \int_{V_{\text{uth}}}^{V_{\text{pth}}} J_m(V) \, dV} \tag{4.30}$$
$$\tag{4.31}$$

where V_{uth} is the 'uniform' threshold, the threshold equivalent to a single patch of membrane. $J_m(V)$ is negative between the resting potential and the uniform threshold, such that any subthreshold current causes the voltage to simply return to the resting potential. Then, the first term of equation 4.30 is necessarily negative and consequently the second term has to be positive to respect the inequality. Assuming we are looking for a $V_{\text{pth}} > V_o$, then $V_{\text{pth}} > V_{\text{uth}}$. This is true if J_m allows such a threshold to exist. For most membranes, the sodium current beyond threshold is so big compared to the currents below threshold, that this criterion is easily met. In other words, the threshold for propagation initiation on an infinitely long axon is higher than the threshold of uniform initiation. [Jack et al., 1975]

The fact that an action potential can't propagate along the axon without nonlinear conduction, i.e. without having its entire surface filled with voltage-gated channels, and the fact that this long conducting membrane requires more current to initiate an action potential, make this simplified uniform axon a very inefficient way to transport the action potential.

This is why most long axons use other ways to initiate and propagate action potentials, as we now discuss.

4.4.3 Myelinated axon

We previously described the myelin sheath. This sheath has the effect of decreasing the conductance and the capacitance of the axon segment underneath it, analogously to a coaxial cable. Nodes of Ranvier periodically interrupting this myelin sheath act as repeaters that counteract the voltage amplitude losses over distance. As a bonus property, the nodes of Ranvier are very short segments and are stimulated virtually uniformly, and so do not have an increased threshold.

The electric isolation of the node is due to the difference between its characteristic impedance and that of the myelinated segment. The characteristic impedance of a segment is given by:

$$Z = \sqrt{\frac{\rho_a}{g - i\omega C_m}} \qquad \text{(Fourier space)} \tag{4.32}$$

$$= \sqrt{\frac{\rho_a}{g + sC_m}} \qquad \text{(Laplace space)}\,. \tag{4.33}$$

The conductance is virtually zero, making its characteristic impedance very large, significantly larger than that of a node's.

4.4.4 The axon initial segment

The axon initial segment we described in the previous chapter seems to not be the most efficient site of action potential initiation, since it is very long compared to the nodes. However, despite its disadvantageous length, the special conical geometry combined with the non-uniform channel distribution makes it the most favourable site of initiation. In section A.1, we reconstruct the cable equation without assuming that the radius and the channel densities are uniform. From equation A.3, a very general nonlinear cable equation, we get a specialized equation for our axon taking into account its specific geometry($A(z) = \pi r(z)^2$

and $p(z) = 2\pi r(z)$):

$$V''(z) + 2\frac{r'(z)}{r(z)}V'(z) - \frac{2\rho_a}{r(z)}J_m(V,z) = 0 \tag{4.34}$$

where $r(z)$ is the radius and $J(V(z),z)$ the total current across the membrane at every point z along the axon. This equation will be used in the next chapter for our numerical simulation.

To understand why the conical geometry helps in the initiation, it is sufficient to look at simple special cases as in appendix A.1. With many changes of variables, one ends up with a solution that has many desirable features for an initiation site: lowered threshold and amplification and extended decay, with these last two properties occurring even for an ohmic membrane conductivity.

The solution on a non-uniform segment of axon can be written

$$V = V_o\left(\frac{r(x)}{r_o}\right)^{-3/4}\left(\frac{\kappa(x)}{\kappa_o}\right)^{-1/4}\left(\frac{g(x)}{g_o}\right)^{1/4}\phi(x) \tag{4.35}$$

where ϕ is solved as a potential on a uniform axon with a change of variable $x = \lambda(x)\xi$ where $\lambda(x)$ is the nonuniform length constant along the segment:

$$\phi'' - (q+1)\phi = 0\,. \tag{4.36}$$

These variables are all defined in section A.1.

Figure 4.3 shows a solution for a conical axon initial segment, with the larger diameter being connected to the soma and the smaller one to the model myelinated axon. One sees the characteristic amplification at the distal points (i.e. points further away from the soma) at later times. This distal amplification is absent from the uniform axon segment case shown in figure 4.4). In the next chapter we investigate full propagating solutions with a healthy initial segment as well as with a damaged initial segment, and draw comparison as a function of the magnitude of the coupled left shift.

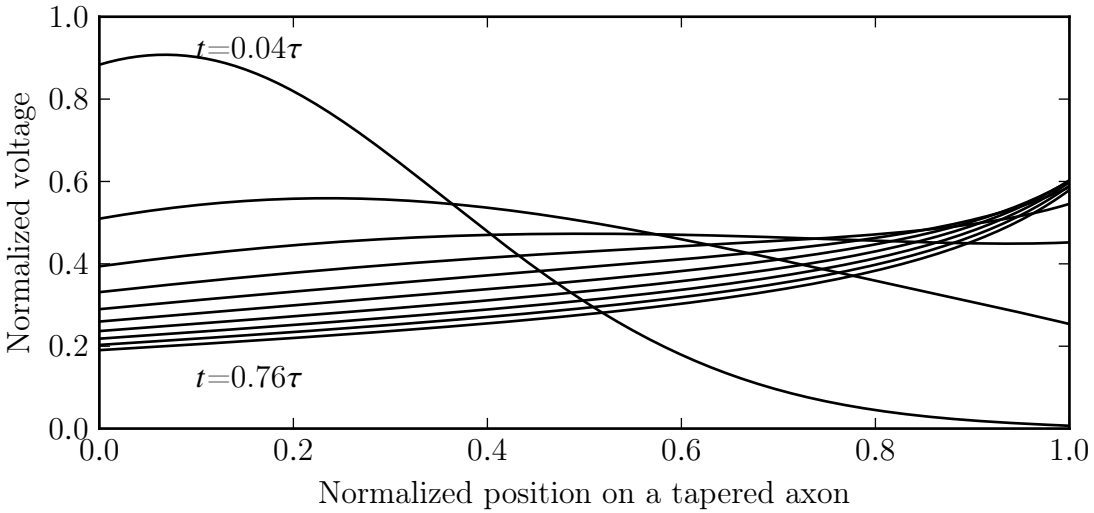

Figure 4.3: *Action potential initiation in a conically tapered axon initial segment.*

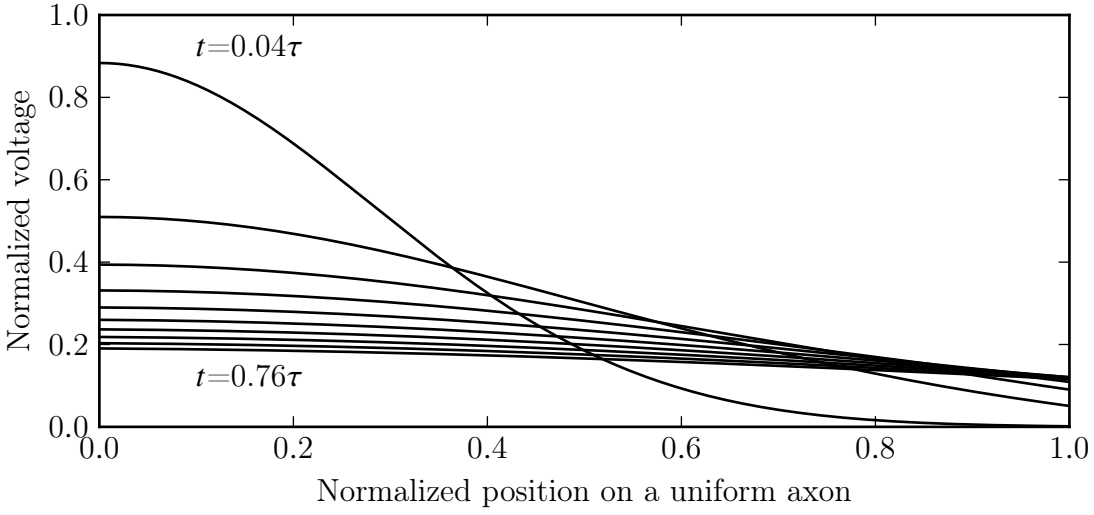

Figure 4.4: *Action potential initiation in a uniform axon initial segment.*

Chapter 5

Numerical Simulations

5.1 Introduction

The previous chapter described the biophysics involved in the initiation of an action potential in an AIS with damaged sodium channels. We mostly concentrated on the length scale of micrometers and time scale of microseconds, but there's enough material to construct a realistic numerical model on which we can simulate basic AP initiation.

We believe that the idea of combining the AIS with CLS damage in the same model is original. However previous separate AIS and CLS studies were an inspiration for designing our own model (see section 2.2). We designed this model with the intention of representing the AIS accurately while keeping simplicity in mind (see section 5.2).

While relying on a limited number of components and concepts, the simulation of this model and the algorithm used to find the initiation threshold of various configurations was computationally intensive(section 5.3). After, confirming that our model was appropriate (section 5.4), we explored the relation between CLS damage and AP initiation on various geometries of AIS and various spatial distributions of damage (section 5.5).

5.2 Model

We modeled our axon using a system of partial differential equations (PDEs) introduced in section 4.4 with the standard HH model from section 4.2.1. This system was solved

numerically using a fourth-order Runge-Kutta method with adaptive time-step. Damage to the AIS was simulated using the CLS model introduced in section 3.3.3. Thus, equations 4.18 and 4.34 together yield:

$$\dot{V}(z,t) = -C_m^{-1}(z)\left(I_{\text{inj}}(z) - \left(\bar{g}_{\text{Na}}(z)m^3(z,t)h(z,t) + \bar{g}_{\text{Na,CLS}}(z)m_{\text{LS}}^3(z,t)h_{\text{LS}}(z,t)\right)(V(z,t) - E_{\text{Na}})\right. \tag{5.1a}$$

$$\left. -\bar{g}_{\text{K}}(z)n^4(z,t)\,(V(z,t) - E_{\text{K}}) - g_{\text{L}}(z)\,(V(z,t) - E_{\text{L}}) + \frac{r(z)}{2\rho_a}V''(z,t) + \frac{r'(z)}{\rho_a}V'(z,t)\right)$$

$$\dot{m}(z,t) = -\tau_m(V(z,t))^{-1}\,(m(z,t) - m_\infty(V(z,t))) \tag{5.1b}$$

$$\dot{h}(z,t) = -\tau_h(V(z,t))^{-1}\,(h(z,t) - h_\infty(V(z,t))) \tag{5.1c}$$

$$\dot{n}(z,t) = -\tau_n(V(z,t))^{-1}\,(n(z,t) - n_\infty(V(z,t))) \tag{5.1d}$$

$$\dot{m}_{\text{LS}}(z,t) = \dot{m}(V(z,t) + V_{\text{LS}}) \tag{5.1e}$$

$$\dot{h}_{\text{LS}}(z,t) = \dot{h}(V(z,t) + V_{\text{LS}})\,. \tag{5.1f}$$

Note that the dot notation refers here to partial differentiation with respect to time in this context of the full spatio-temporal model.

Geometry of the simulated axon

Our goal is to create a simulation of the AIS that reproduces with sufficient detail the initiation of the action potential. To accomplish this goal, we could model only the AIS alone if it were not so tightly coupled to the other segments of the axon. For this reason, we chose to model a length of myelinated axon following the AIS to serve as a non-linear boundary condition in which the initiated AP can start propagating, thus helping us to better define a realistic initiation. At the other extremity of the AIS, a passive soma was included to serve as an injection site as in [Brette, 2013].

The myelinated segments and the soma were simulated with only passive conductances and capacitance. The myelinated segments were kept at the radius of the distal AIS ($r = .5$ μm) but were given a significantly reduced capacitance to account for the thickness of the myelin. The nodes of Ranvier are very short segments ($l = 1$ μm) of unmyelinated membrane on which the standard parameters of the HH model are applied. Finally the axon initial

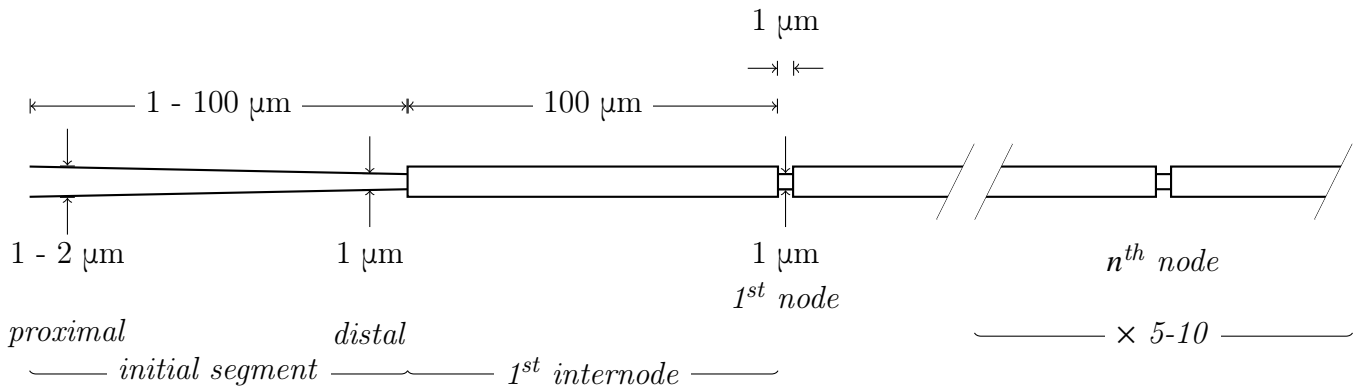

Figure 5.1: *Geometry of the simulated axon*

segment is modeled as a very stretched out node up to 100 µm in length. Parameters are either kept uniform throughout the AIS or are varied linearly between its two extremities. Those are identified as the proximal part connected at the soma and the distal part connected at the first segment of myelinated axon. Figure 5.1

The discretization of each segment was made automatically by sub-dividing them until the outcome of the simulation wasn't affected ($\leq$ 0,1%) by more division. To allow for a good spatial description, a minimum of seven compartments was also set as a condition for the AIS segment.

PDE vs. Multicompartment approach

We model the axon using a system of partial differential equations. The PDE approach is similar and in many cases virtually identical to the multicompartmental approach as solving the system requires the space to be divided in compartments. However, in the former case the resulting compartmentalization is optimized for computational accuracy rather than conceptual simplicity for the latter. For example, most myelinated axon models use multiple compartments assigning one for each Node of Ranvier, lumping together all the surrounding elements in a single element and linking those elements by a simple conductor. The PDE approach would require a spatial description of the node as well as the internodes with their distinct channel distribution and increased capacitance. Some model go as far as to include the periaxonal space(very thin space between the myelin and the axon own

Variable		Soma	Proximal AIS*	Distal AIS*	Myelinated Axon	Node	Units
Radius	r	2.	.5 - 1.0	.5	.5	.5	[μm]
Capacitance	C_m				0.01		[μFcm^{-2}]
Na cond.	$\bar{g}_{\mathrm{Na}}$	0.			0.		[mScm^{-2}]
CLS Na cond.	$\bar{g}_{\mathrm{Na,CLS}}$	0.			0.		[mScm^{-2}]
K cond.	$\bar{g}_{\mathrm{K}}$	0.			0.		[mScm^{-2}]
Leak cond.	g_{L}	10.			0.01		[mScm^{-2}]
Damage distribution							
100%, uniform	γ	0.	1.0	1.0	0.	0.	
50%, uniform	γ	0.	0.5	0.5	0.	0.	
50%, proximal	γ	0.	1.0	0.0	0.	0.	

*Table 5.1: Geometric parameters of simulated axon. This table only shows values that differs from table 4.1. *Values in the AIS varies linearly from values defined for the proximal AIS to values defines for the distal AIS*

membrane) [Dimitrov, 2005]. A multicompartmental model is often perfectly adequate and matches the experimental results [Fitzhugh, 1962]. However, as we want to get a spatial description of the initiation of the action potential, the PDE approach is needed.

5.3 Method

Detection of the initiation

All simulation performed on our axon is an attempt to illicit an action potential. We decided to define a successful initiation of an AP as an excitation of the soma which propagates completely to the end of the myelinated axon. This allows us to ignore the ill-defined threshold in a single compartment HH model as discussed in section 4.3.2.

We define the threshold of initiation as the minimum voltage instantaneously applied to the soma which causes a successful initiation. This voltage is applied with a very short pulse at the soma (Δt = 0.01ms). As illustrated in figure 5.2, we converge to a precise value for the threshold by running the simulation multiple times with a given pulse strength until the pulse strength is close enough to the threshold. The increment and decrement are decided with a bisection algorithm slightly modified to account for cases when the initial excitation is too far from the threshold. In each run, we collect information about the initiation delay, when present. This algorithm becomes very time consuming as the precision requirement for

the threshold increases because the closer the injected pulse is to the threshold, the longer it takes for the AP to initiate as shown in 5.5. Some search for a threshold can take up to two hours but takes around 20 minutes in average. We collect information on the initiation delay as a function of the initiation voltage at the soma.

In section 5.4.2, we also found a way to predict the timing of delay initiation in a single compartment model. We are using this model to fit the experimental data.

Varying the degree of damage and AIS length

The threshold for AP initiation is found using the aforementioned algorithm for a range of coupled left shift of a selected population of Na_V channels and AIS geometry starting from 5 mV with increments of 0.5 mV up to V_{ef} until spontaneous firing is detected. With an extrapolation using the last points where initiation is possible, an estimate of the critical value V_{ef}.

The previously described series of simulations over a range of CLS damage is done on many versions of the axon but with different AIS lengths. The lengths simulated are 5 µm, 10 µm, 25 µm, 50 µm and 100 µm.

5.4 Validation

5.4.1 Initiation at the AIS

A sharp initiation is a key feature of the action potential in a typical cortical neuron [Brette, 2013]. This effect is present in our model, as shown in figure 5.3. As we didn't modify the kinetics of the sodium channel by adding features such as cooperativity [Naundorf et al., 2006], we can attribute it to the separation of the injection point from the initiation along the axon as in [Brette, 2013]. The presence of the special kink in the initiation is clearly present in the nodes to a greater degree.

The initiation, the nonlinear increase in voltage, happens quicker at the distal part of the AIS. As illustrated in figure 5.4. This is consistent with many previous experimental and numerical observations. This is often interpreted as an evidence that action potential

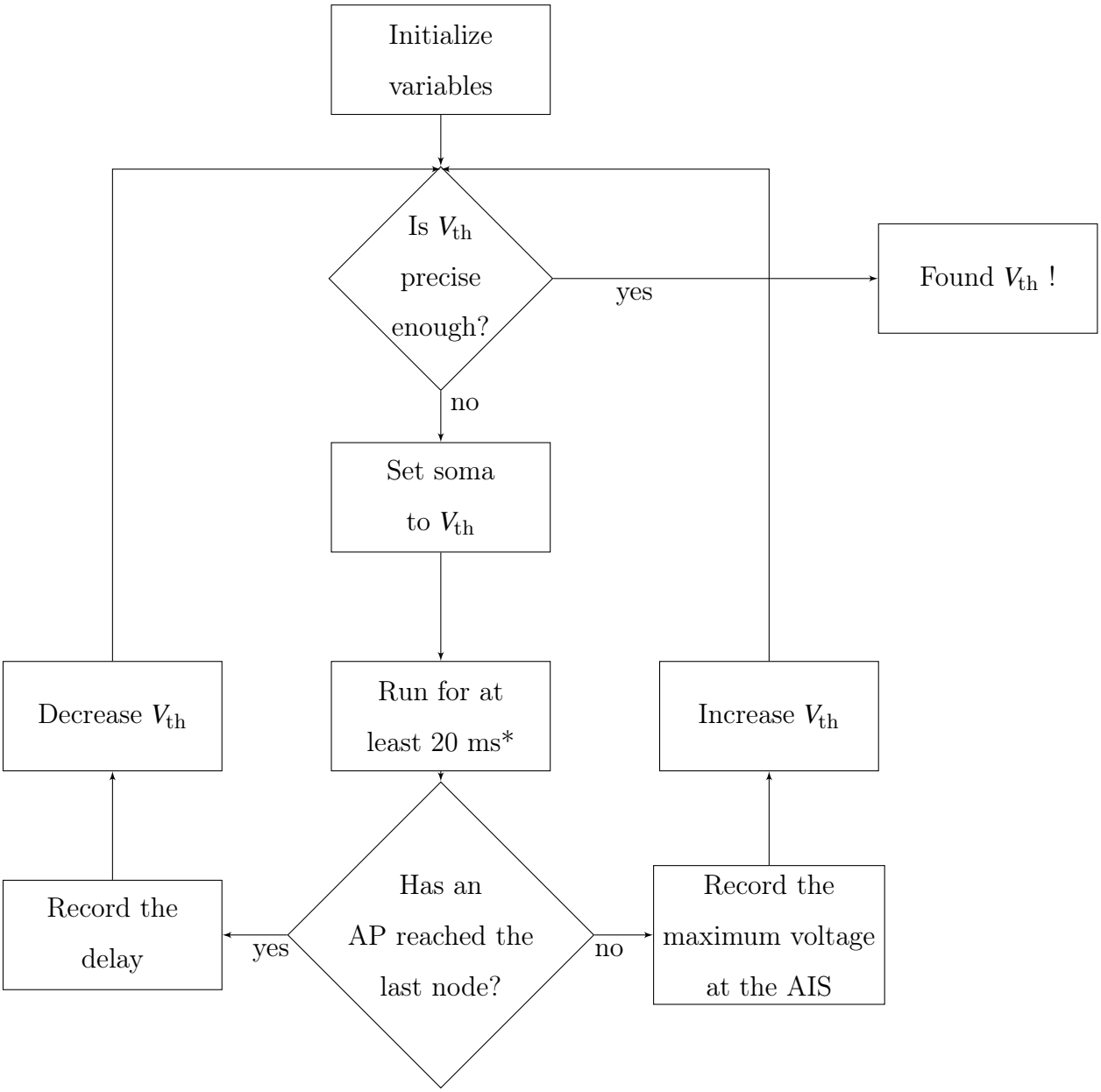

Figure 5.2: *Flow chart of the initiation current threshold finding algorithm. *No initiation was found to take longer than 20 ms.*

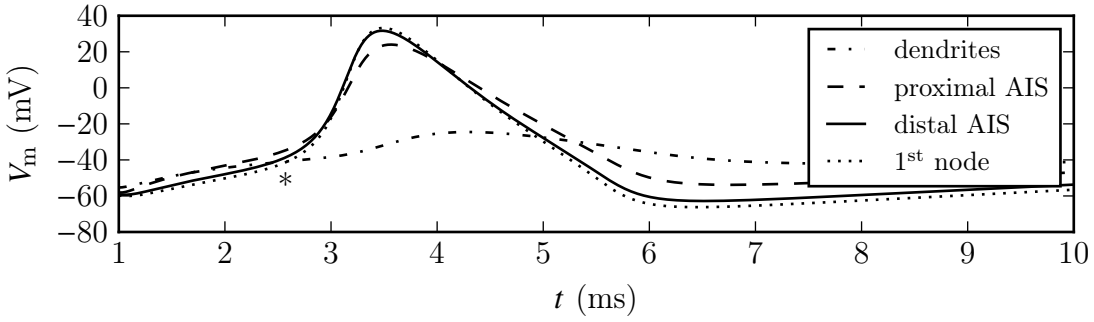

Figure 5.3: *Sharp initiation of the action potential at the AIS from a step current at the soma. The * marks the kink missing from single compartment HH models. The action potential appears first in the distal part of the AIS and followed closely by the the first node and later backpropagates in the proximal AIS and the soma.*

initiates at this point. The delay between the different initiations on different parts of the initial segment, on the order of microseconds, is very short and might have negligible direct effects on the initiation or other activities at the AIS. However, this 'initiation site' is a feature easy to measure and can be used to describe the initiation, a change of it's location or timing could help describe the change of the AIS itself.

5.4.2 Initiation delay close to the initiation threshold

In section 4.3.2, the initiation from a pulse on a single segment was described using a simplified model containing only a dynamic saddle-node bifurcation. As described in 5.3, in the process of finding the initiation threshold many initiations are tested close to the initiation threshold. If the delay observed fits the equation 4.23, then the parameters could also reveal important changes in the dynamics of the initial segment when damaged.

In figure 5.6, we observe that the initiation delay does follow our theory very closely and reveals that our approximation is still valid for the AIS. For each set of parameters of the AIS, we will use the information from this linear fit to characterize the initiation. A steeper slope indicates a robustness of the initiation delay, i.e. changes in the excitation amplitude will have a lesser effect. The y-intercept represents the delay of initiation and propagation for an infinitely strong stimulus.

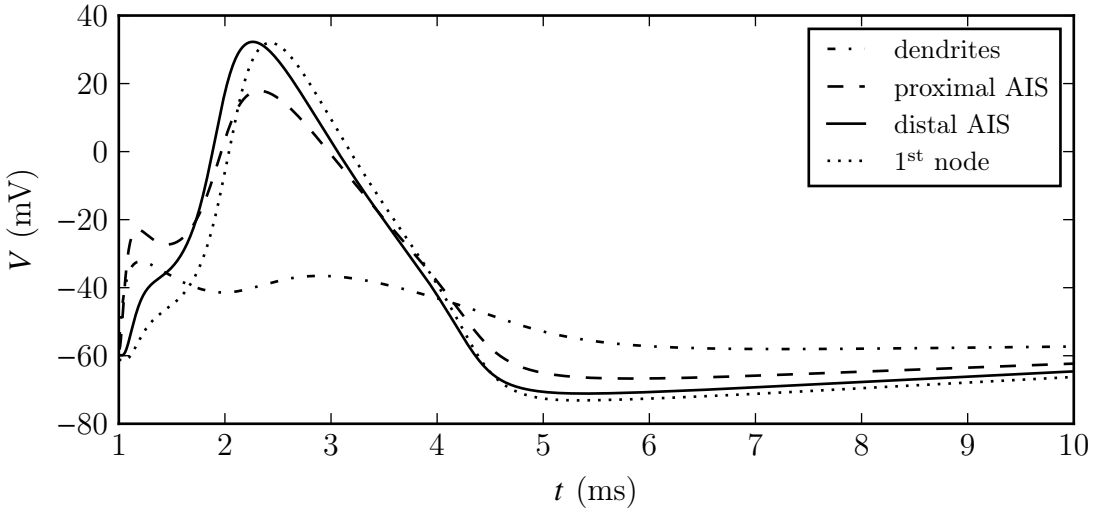

Figure 5.4: *Sharp initiation of the action potential at the AIS from a very short pulse current at the soma($\Delta t = 0.01$ms). In comparaison with figure 5.3, the initiation happens at different time for different locations on the axon.*

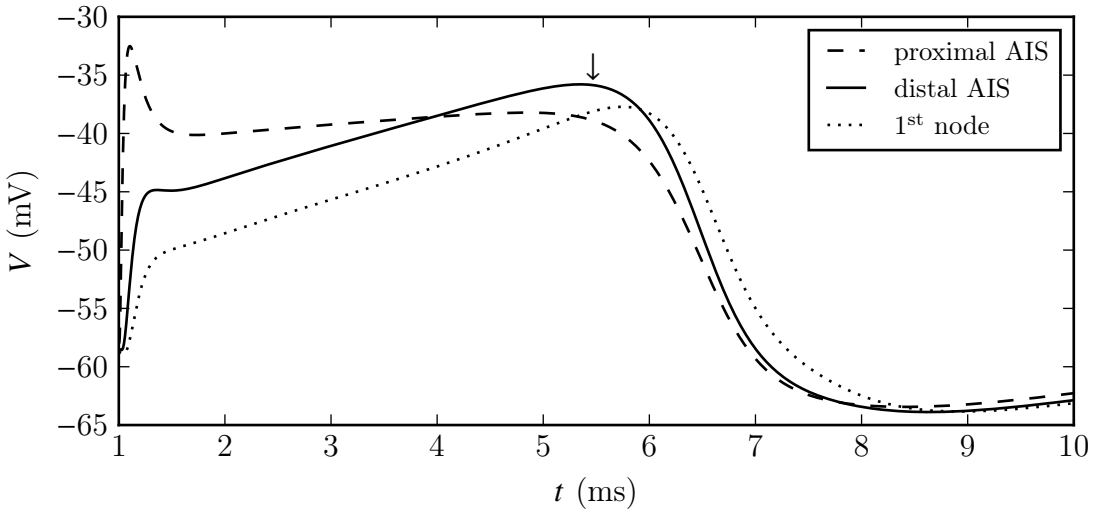

Figure 5.5: *Sharp initiation of the action potential at the AIS from a very short pulse current at the soma($\Delta t = 0.01$ms), just below threshold. The arrow points to the maximum voltage which is at the distal part of the AIS*

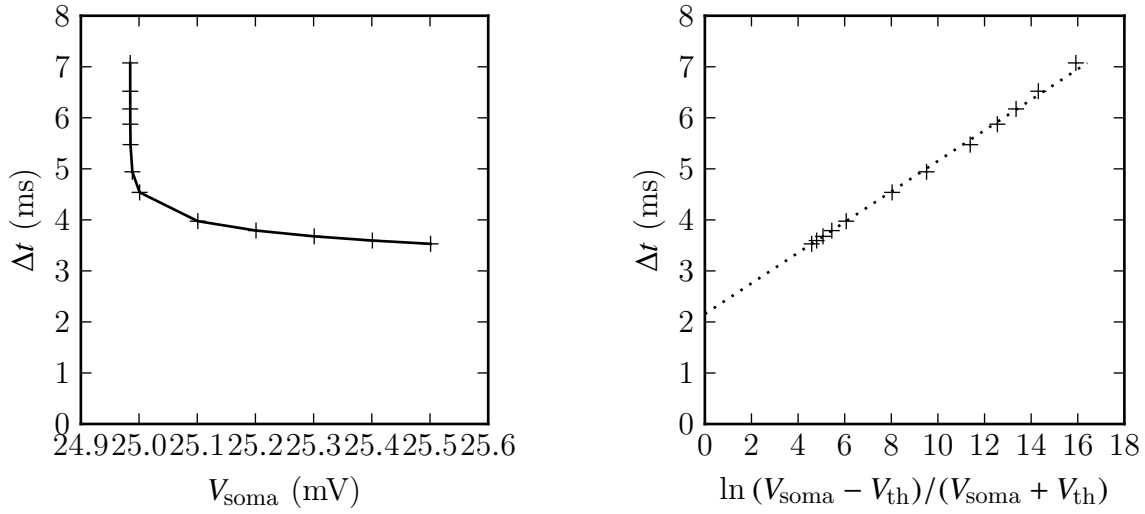

Figure 5.6: *Delay of initiation near the current threshold for initiation. The figure on the left is the delay between the injection and the detection an AP at the last node. The figure on the right is the same data but fitted on our model for initiation delay.*

5.5 Results

In figure 5.7, we affected all the sodium channels of the AIS on axons of different AIS lengths. The AIS threshold decreases with increasing V_{LS} but also with decreasing length. We notice an inversion of the relation between the length and threshold at around $V_{\mathrm{LS}} \approx 6\mathrm{mV}$. The axons exhibit spontaneous firing after around $V_{\mathrm{LS}} \approx 8\mathrm{mV}$ for longer AIS and $V_{\mathrm{LS}} \approx 12\mathrm{mV}$ for the shortest.

In figure 5.8, we repeat the same experiment but with only half of the channels affected uniformly throughout the axon. We notice the same inversion but at a higher value of $V_{\mathrm{LS}}(\approx 8.5\mathrm{mV})$. The axon starts firing spontaneously for higher damage ($V_{\mathrm{LS}} \approx 10\mathrm{mV}$. From the timing information, we gather the initiation delay and the sensitivity of the delay to variation of the applied voltage shown in figure 5.9 and 5.10, respectively. We notice the minimal delay varies only slightly except for smaller AIS close to the spontaneous firing limit where it increases significantly. The sensitivity of the delay to variation of the stimulus shows a significant increase close to the spontaneous firing limit where longer AIS are more affected than shorter AIS.

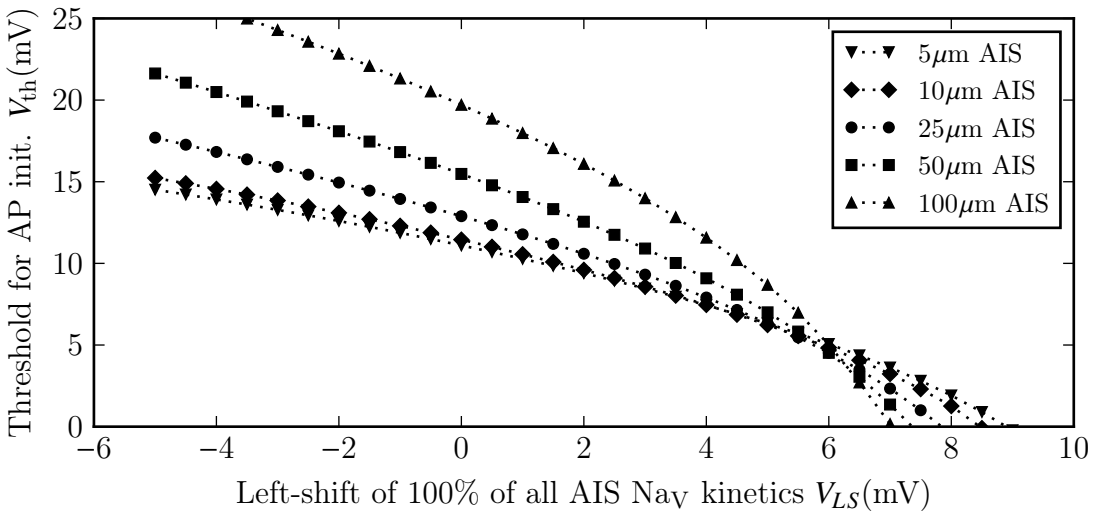

Figure 5.7: *Initiation threshold of axons with all the voltage-gated sodium channels affected uniformly by a couple left-shift of their gating dynamics. The threshold decreases with the CLS and finally reaches spontaneous firing between* 7mV *and* 9mV *for longer and shorter AIS respectively. The threshold increases with the size of the AIS until an inversion after* ~ 6mV

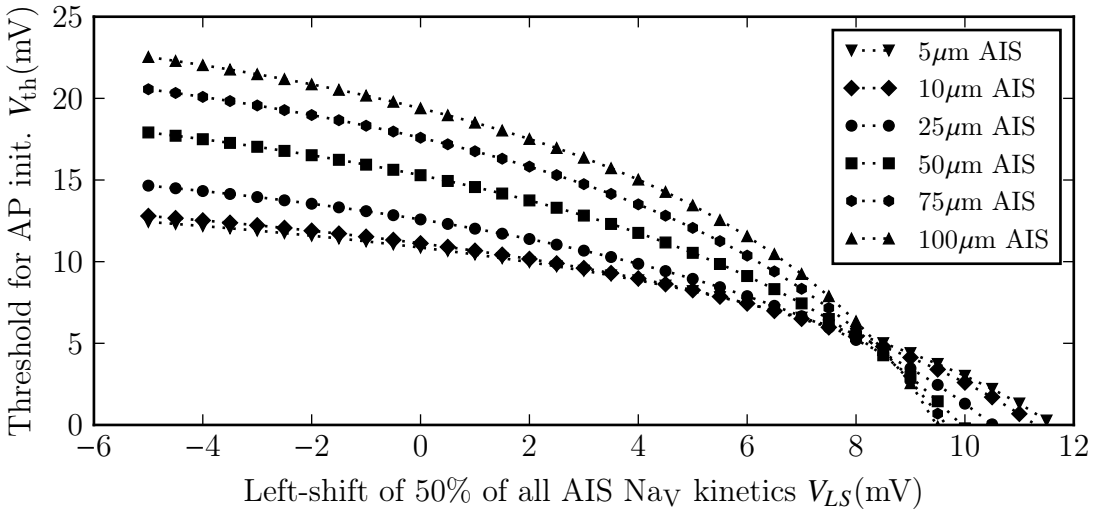

Figure 5.8: *Initiation threshold of axons with* half *the voltage-gated sodium channels affected uniformly by a couple left-shift of their gating dynamics. The threshold decreases with the CLS and finally reaches spontaneous firing between* 9.5mV *and* 12mV *for longer and shorter AIS respectively. The threshold increases with the size of the AIS until an inversion after* ~ 8mV

Figure 5.9: *Delay of initiation for a very large stimulus on different sizes of axon and at different degrees of damage on half of the AIS Na_V channels. The dependence on the left-shift is small except for the shortest AIS. The dependence on the length is also small except close to spontaneous firing limit or for negative left-shifts where shorter AIS has their initiation delay increase with damage.*

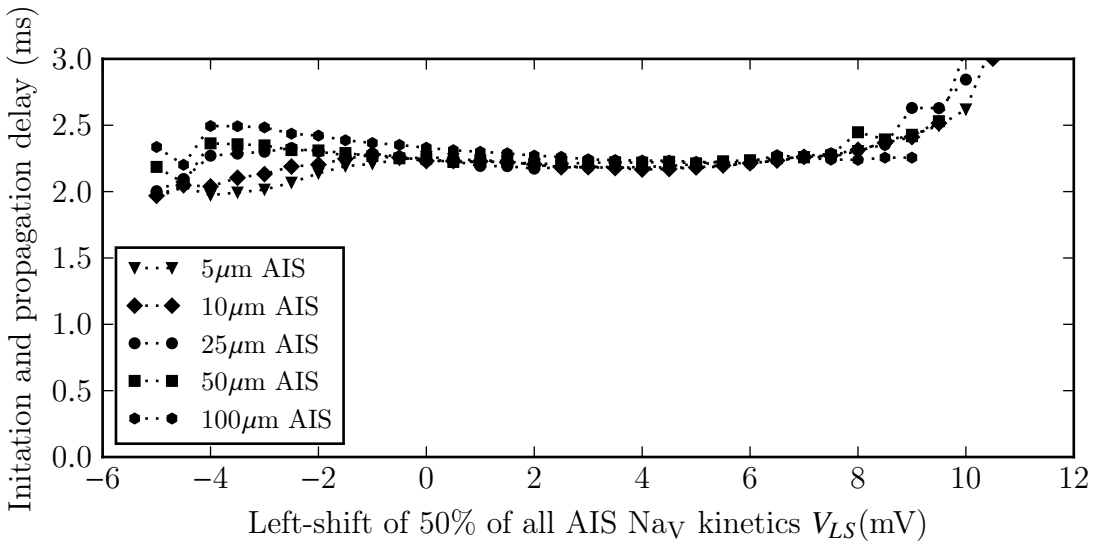

Figure 5.10: *Sensitivity of the delay to variation applied voltage for a very large stimulus on different sizes of axon and at different degrees of damage on half of the AIS Na_V channels. In this case, initiation delay in longer AIS are more affected with variation in the stimulus than shorter one.*

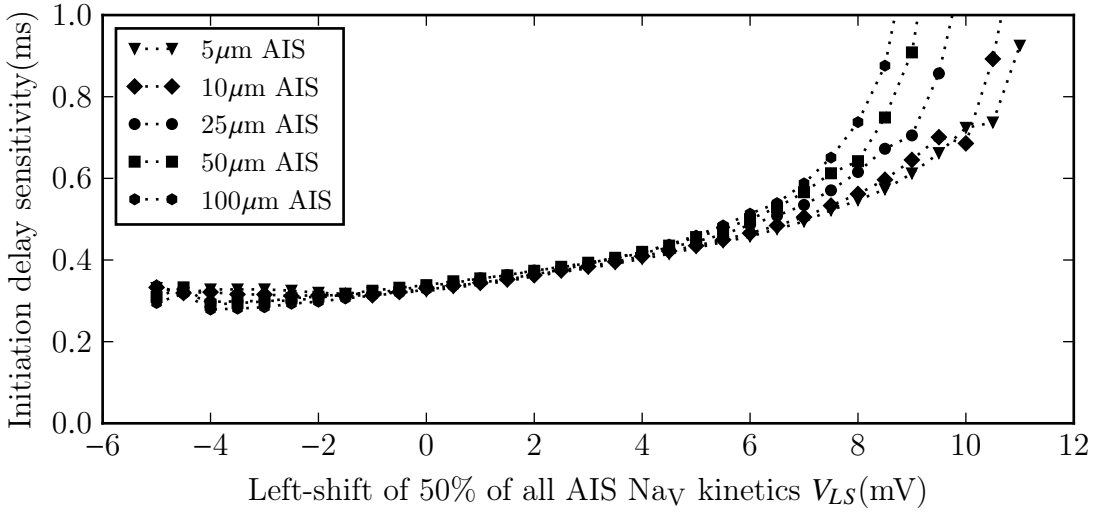

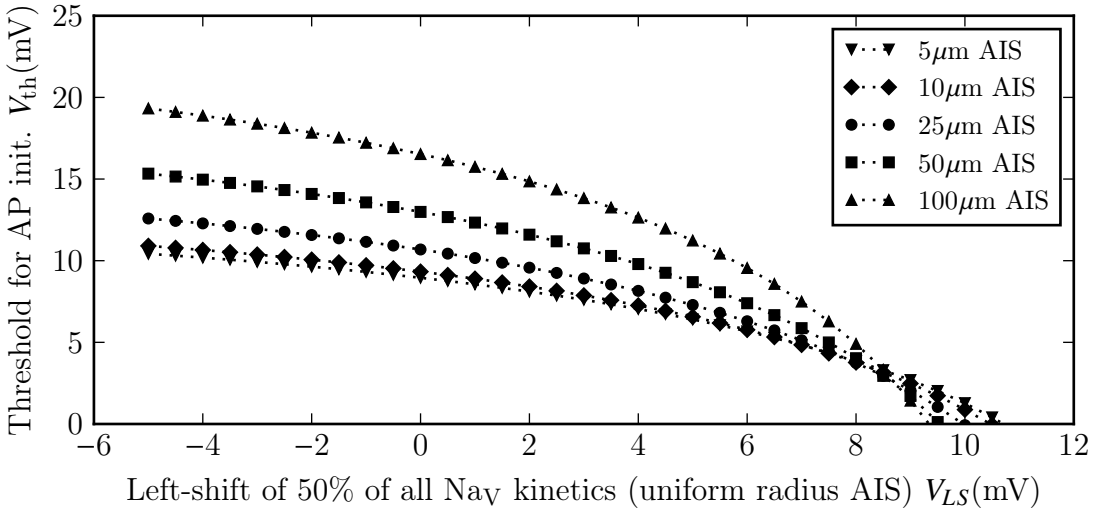

Figure 5.11: *Initiation threshold of axons with half the voltage-gated sodium channels affected at the proximal part of the AIS by a coupled left-shift of the gating dynamics. The diameter of the AIS is kept constant on its entire length. This figure mostly differs from figure 5.8 only by a factor of* ~ 0.83 *for values not too close to the spontaneous firing limit.*

We note that as the radii of the distal and proximal segments of the AIS are fixed to 0.5 μm and 0.75 μm respectively, the effects to the initiation threshold of a steeper taper and a shorter length combine. To separate those effects, we repeat the previous experiment, with half the sodium channels affected, but with an axon with uniform radius instead. The results in figure 5.11 shows us that the threshold is only different by a factor of ~ 0.82 while other features of the threshold curves are identical. Significant differences are present in the delay. In figure 5.12 and 5.13, the dependence on the length in the case of the tapered axon, albeit small, almost completely disappears.

In figure 5.14 we repeat the previous experiment by applying the coupled left-shift of the kinetics on the proximal part of the tapered AIS. This redistribution of channels was made ensuring that the total number of channel was conserved by taking into account the decreasing area along the AIS created by the taper. The inversion of the length-threshold current relation happens for greater left-shift ($V_{\mathrm{LS}} \approx 8.5\mathrm{mV}$) but the spontaneous firing happens for sligthly lower values than in the uniformly damaged case ($V_{\mathrm{LS}} \approx 9\mathrm{mV}$)

Figure 5.12: *Delay of initiation for a very large stimulus on different sizes of axon and at different degrees of damage on half of the AIS Na_V channels, on an axon with uniform radius. The dependence on the left-shift is small except for the shortest AIS. The dependence on the length almost completely disappeared compared to figure 5.9, indicating that it was actually a dependence on the slope of the taper of the AIS rather than the length itself.*

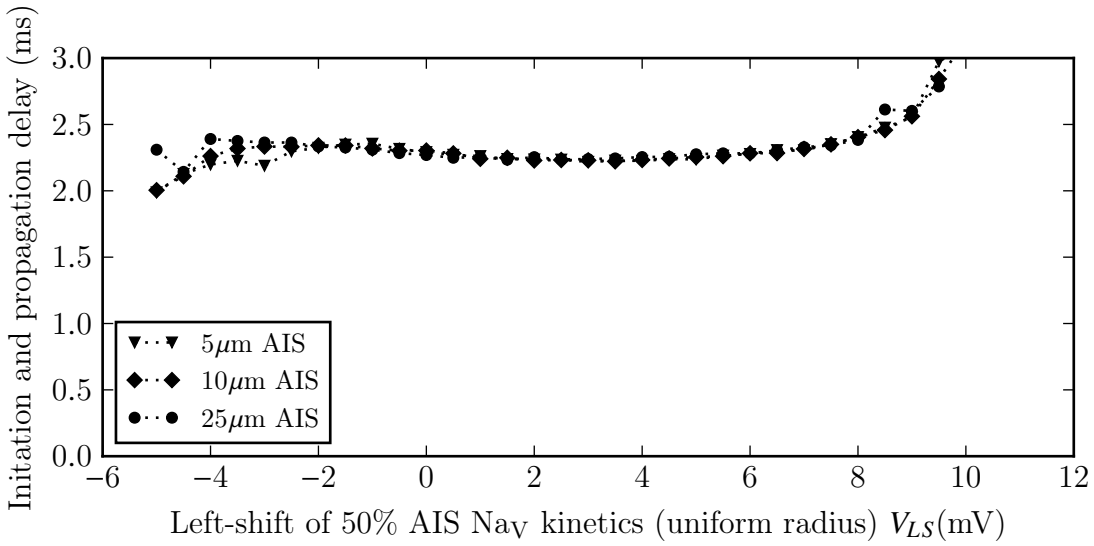

Figure 5.13: *Sensitivity of the delay to variations in the applied voltage for a very large stimulus on different sizes of axon and at different degrees of damage on half of the AIS Na_V channels, on an axon with uniform radius. As in 5.12, the dependence on the length almost completely disappears.*

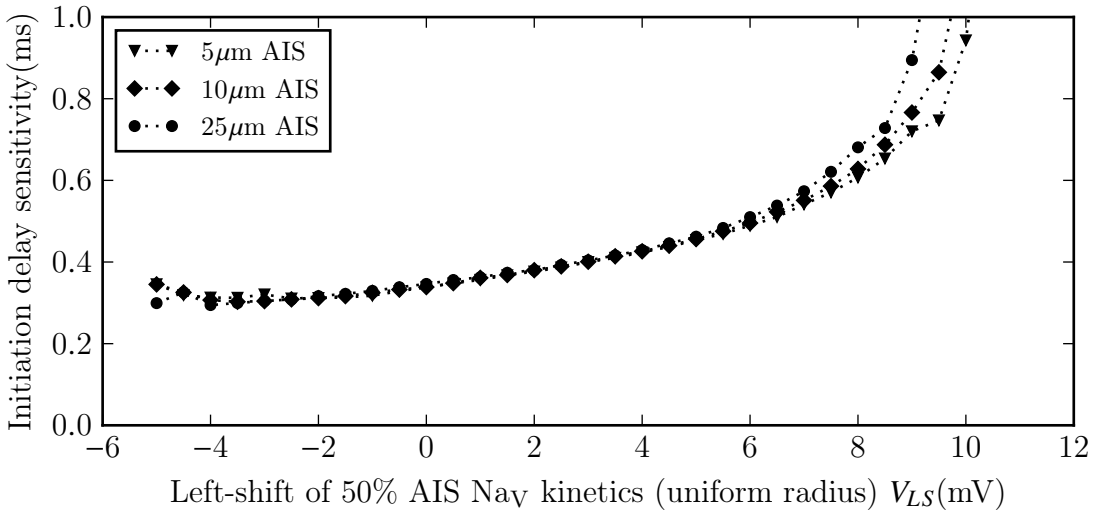

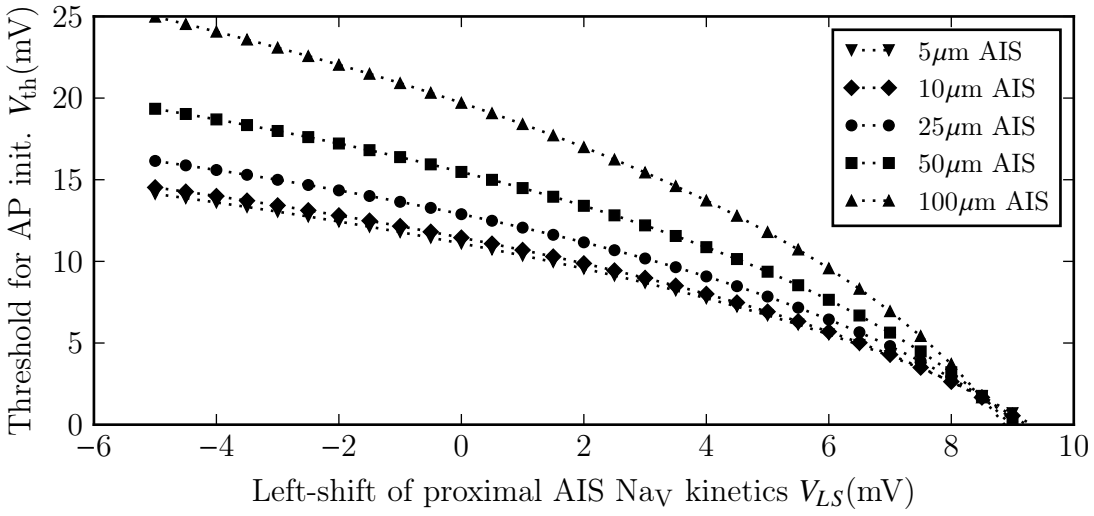

Figure 5.14: *Initiation threshold of axons with the Na_V channels affected by CLS at the proximal part of the AIS and the distal channels kept intact. The threshold is almost as high as for the axon with all Na_V damaged, especially for shorter AIS. The inversion of the relation between the size and the threshold is happening around the critical V_{LS} for spontaneous firing*

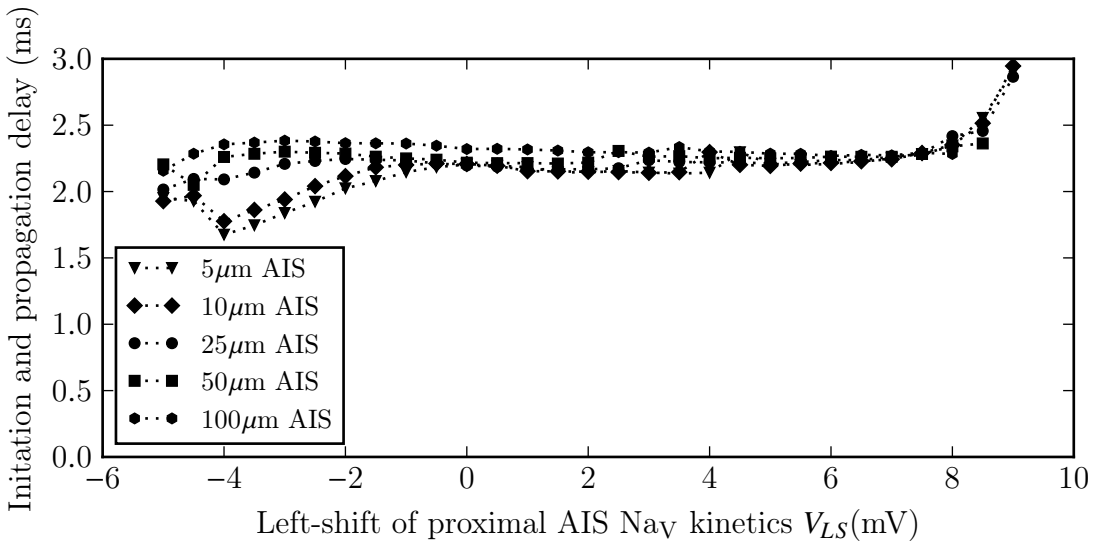

Figure 5.15: *Delay of initiation for a very large stimulus on different sizes of axon and at different degrees of damage on the proximal AIS Na_V channels while keeping the distal AIS Na_V channels intact. This figure is qualitatively similar to 5.9 with a slightly greater variance due to the length of the AIS.*

Figure 5.16: *Sensitivity of the delay to variations in the applied voltage for a very large stimulus on different sizes of axon and at different degrees of damage on the proximal AIS Na_V channels while keping the distal AIS channels intact.*

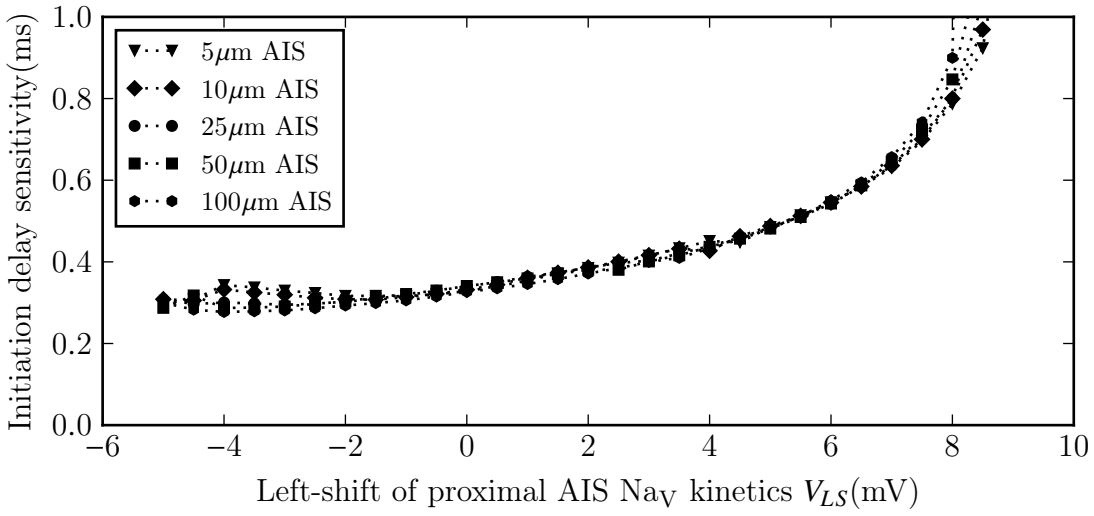

5.6 Discussion

In this study we have shown that damage to sodium channels of the axon initial segment changes the action potential initiation properties. One important affected property is the activation threshold that has unambiguously decreased with increased damage. We also studied in detail the timing of the initiation related to the strength of the activation. We found that the geometry had an important role in the activation delay, accounting for most of the variance for small left-shift. We also found that, despite the AIS being a relatively small compartment, the localization of the affected channels plays an important role in how much the damage will affect the axon. While testing the system we also reconfirm the localization of the initiation site.

5.6.1 Coupled left-shift of Na_V channels lowers the initiation threshold

The most obvious result in these simulations is the apparent lowering of the initiation threshold with the left shift of the Na_V channels. This doesn't come as a surprise as one of the

affected gating variables, m, is commonly called the 'activation gate'. By making the open probability greater for lower values of transmembrane voltage, we require less charge to activate this gate, and then initiate the AP.

Another contributing consequence of the left-shift, is the change in the resting potential. We saw previously that an unstimulated membrane equilibrates to a given voltage depending on its ionic conductances and corresponding resting potentials. Increasing the sodium conductance will bring this resting potential closer to the positive reversal potential of sodium ions. When this resting potential is well into the 'window conductance', it fires spontaneously, and even continuously if no adaptation is present. This systematically happens in our simulations when the left-shift approached 10mV.

5.6.2 Longer initial segment requires greater charge for initiation

An important observation is the relation between the threshold and the length of the AIS. In the healthy case ($V_{LS} = 0$), the increase in excitability is always proportional to the size of the AIS. This seems to go against the observed fact that longer AIS have shorter spiking frequency [Baalman et al., 2013]. However, the axons in our simulations were excited with pulses instead of step currents. We can retrieve the usual negative proportionality between the length and the excitation, whatever its type, when the damage is high enough to spontaneously fire. A step current applied to a membrane acts as a shift to all its kinetics. When this shift is high enough, the membrane fires spontaneously and gives the usual spike train. Our results show that in the case of spontaneous firing, longer AIS are more sensitive than shorter ones.

To explain the length-excitation relationship in the case of the healthy axon, we consider the soma, the injection site, and the AIS, the initiation site, as two separate compartments connected in parallel made of a capacitor and a conductor also in parallel. By applying a very short pulse to the soma, we charge its capacitor very rapidly. From this point, the charge has to distribute equally between those two compartments, trying to get their voltage to be the same. The total capacitance now includes the AIS's which proportional to its surface area. Therefore a bigger AIS will require a greater initial charge at the soma to get the same voltage as a shorter AIS. The voltage is what triggers the gating variables, not the

current. This relation between the voltages at the soma and the AIS can be explained by the following equation relying on conservation of charges.

$$
\begin{aligned}
Q_{\text{soma}}(t=0) &= Q_{\text{soma}}(t\to\infty) + Q_{\text{soma}}(t\to\infty) \\
A_{\text{soma}}C_{\text{soma}}V_{\text{soma}} &= (A_{\text{soma}}C_{\text{soma}} + A_{\text{AIS}}C_{\text{AIS}})V \\
V &= \frac{A_{\text{soma}}}{A_{\text{soma}} + A_{\text{AIS}}}V_{\text{soma}} \\
&= \frac{A_{\text{soma}}}{A_{\text{soma}} + \pi(r_{\text{prox.}} + r_{\text{dist.}})}V_{\text{soma}}
\end{aligned}
$$

where A_{soma} and A_{AIS} are the membrane areas of the soma and the AIS respectively. We assumed the capacitance per area to be the same in both compartment.

5.6.3 Spatial distribution of channels helps with boundary conditions

Now to explain the inversion in the length-threshold relationship, we point out that our previous explanation omitted the rest of the axon. We didn't count the charges accumulated in the myelinated axon. When the charge is allowed to leak in the myelinated axon, a shorter AIS will give less total axial resistance and then might not keep the charge long enough to reach a voltage high enough to initiate. The question is what would increase the charge leak in the rest of the axon in one case and not in the other. Comparing the impedances of the AIS (Z_{dAIS}) and the myelinated axon ($Z_{\text{Myel.}}$), we find that there's a big mismatch, leading to a lot of reflection of signal at their junction. Assuming the myelinated axon has no transmembrane conduction and that the axoplasm has constant resistivity and radius, we can look at the reflection coefficient at small frequency:

$$
\begin{aligned}
R &= \frac{Z_{\text{Myel.}} - Z_{\text{dAIS}}}{Z_{\text{Myel.}} + Z_{\text{dAIS}}} \\
&\approx 1 - 2\sqrt{i\omega\frac{C_{\text{Myel.}}}{g_{\text{dAIS}}}}
\end{aligned}
$$

At rest, the reflection is total. Once the AIS charges, higher frequencies appear and lower the reflection, allowing propagation. We note that g_{dAIS} in this case is the differential

conductance, or "slope conductance" and therefore can be lower or even negative even when the actual current is high. This happens when the membrane is near the threshold. When the action potential is initiated the membrane reverses its current, i.e. has a negative differential conductance and at a point a zero differential conductance (the saddle-node bifurcation often discussed). Near this point, g_{dAIS} is low enough to allow signals of lower frequencies to leak in the myelin. A step current as well as a shift in the channels' kinetics can help put the AIS closer to this axial leaking state into the myelin. In our simulation, excluding damage from the distal part AIS made the inversion of the length-threshold relation happen for greater damage relative to the spontaneous firing limit (see figure 5.14). Furthermore, variation in the timing properties were minimal near threshold compared to the uniformly damaged case.

This interpretation of the relation between the length of the AIS and the initiation threshold leads us to conclude that the membrane conduction properties near the boundaries are important. The AIS is electrically very short, mostly shorter than its space constant, making a nonuniform distribution requiring expensive molecular mechanisms seem impractical. However, the impedance matching relies on the electrical properties at the boundaries. Therefore, having specialized channel densities at both ends could be more influential in timing the propagation(and backpropagation) than changing its threshold [Hu et al., 2009].

5.6.4 Coupled left-shift of Na_V channels decreases the delay of initiation and increases its dependence on the stimulus strength

Our simulations mostly tested stimuli close to the threshold. Our analysis of the abnormally long delays in these initiations lead us to fit them to simplified models of initiation(section 4.3.2). The parameters extracted from the fit were interpreted as the minimal delay possible for the y-intercept, and a measure of the sensitivity of the delay to change in stimulus strength for the slope.

We found that this minimal delay doesn't really change with the left-shift(see figures 5.15, 5.9 and 5.12). However, this minimal delay requires an infinitely strong stimulus. The delay from a normal stimulus would be longer than the minimal delay with an increase proportional to this sensitivity parameter. This parameter changes significantly with the degree of left-

shift in the sodium channels. In the context of a normal stimulus on a damaged AIS, a given stimulus would give a retarded initiation by delay of the order of 0.1ms. This could have important effects in any part of the brain relying on precise synchronization, such as coincidence detection [Kuba et al., 2006].

5.6.5 The distribution of the damaged sodium channels affects the timing of the initiation

Looking at figure 5.10, we notice that past a certain damage, the sensitivity of the delay to change in the stimulus strength is less important for shorter AIS. However, in figure 5.16 where the distal Na_V were kept intact, the sensitivity doubles close to the spontaneous firing limit regardless of the AIS length. This is consistent with our previously discussed importance of the distal Na_V channels in timing the propagation into the myelinated axon. An overall increase in the left-shift of the channels will increase the delay sensitivity to stimulus variation, but there's a counteracting effect related only to the distal channels.

Chapter 6

Conclusion

This thesis aimed at describing the effect of damaged sodium channels in the axon initial segment on the action potential initiation. The analysis of our numerical simulations showed us many significant consequences of altered sodium gating dynamics on the properties of the initiation. We observed that the axon became hypersensitive with increased damage. We also observed that this effect was dependent on the geometry of the axon initial segment. A longer AIS, with higher initiation threshold when healthy, was more affected by damage to its sodium channels. While studying the spike initiation threshold, we observed an influence of the damage on the timing of the initiation following stimulation. Not only did the initiation became faster as the threshold lowered, but the mutual dependence between the initiating stimulus strength and the timing increased. We also found a significant influence of the location of the damage on this increase in timing sensitivity. Further, damage localized to the proximal part of the AIS had less influence on the timing than when it was distributed uniformly along the AIS.

While constructing the model for studying the effect of damage, we also studied the theoretical influence of the AIS geometry on its electrical properties. We found that a decreasing radius had a great influence on determining the precise site of initiation at the distal part of the AIS. This was a consequence first of the amplification of the membrane voltage as the current flows in a reduced conductor, and secondly, of the effective reduction of the threshold. The numerical simulations were made using partial differential equations, rather than with a small number of discrete compartments. This enabled us to accurately

model continuous changes in the geometry of the AIS.

To analyze the timing of spike initiation following stimulation, we relied on a simplified theoretical model of initiation in a single compartment. The fit was surprisingly good despite the complexity of the AIS. We are confident that the conclusions made from this analysis are at least qualitatively valid. Nevertheless, the partially phenomenological model still requires a more rigorous foundation to better interpret the results and recommend its applicability to a range of phenomena.

Much work is also still needed to understand the channel damage in the AIS. First we need to investigate and potentially expand the model to account for phenomena on longer time scales. And to look further than the initiation, a complete model of the ion concentration dynamics would need to be established. An understanding of the astrocytes, which support the activity of neurons by regulating their ionic milieu, as well as of the volume compartmentalization in the brain (especially in the dense spaces around neurons), would probably be essential, as they are key determinants of ion concentration gradients (which determine the reversal potentials for the sodium and potassium currents).

Future work would also need to take into account the spatial complexity of the AIS and the rest of the axon. In fact, the AIS is more than a simple cone. And additional geometric features of the axon could have important effects. The distribution of the channels was very simplified in our model and we ignored the separation of potassium and sodium channels in the nodes. In the other direction, a simpler model is also needed. We need a realistic, single compartment model for the AIS. It would allow faster simulations and easier integration to other multi-compartmental models, and perhaps a better analytical handle on how the biophysical features of the AIS control its excitability.

Appendix A

Mathematical derivations

A.1 Non-uniform cable equation

We want to construct a cable equation including nonuniform radius, geometry and conductance, with otherwise simple assumptions. We start with ohm law's for the axial currents I_z,

$$\begin{aligned} V'(z) &= -R_a(x) I_z(z) \\ &= -\frac{\rho_a}{A(z)} I_z(z) \end{aligned} \tag{A.1}$$

where ρ_a is the axoplasmic resistivity, assumed constant, and $A(z)$ the cross-section area varying along the axis of the axon.

We include the continuity equation, any change in the axial current is due to transmembrane current density

$$I_a'(z) = p(z) J_m(V, z) \tag{A.2}$$

where $p(z)$ is the perimeter of the cross section and $J_m(V, z)$ is the transmembrane current density. We omitted the distinction between the external and internal current, we assume them to be the same but with opposite signs. V is the internal voltage; the external volume is considered as a ground (and thus zero) and I_z is the internal axial current. Combining

equations A.1 and A.2,

$$\begin{aligned} V'' &= -\rho_{\mathrm{a}}(\frac{1}{A}I_z)' \\ &= -\rho_{\mathrm{a}}\left(-\frac{A'}{A^2}I_z + \frac{1}{A}I_z'\right) \\ &= -\rho_{\mathrm{a}}\left(-\frac{A'}{A^2}\left(-\frac{A}{\rho_{\mathrm{a}}}V'\right) + \frac{p}{A}J_m(V)\right) \\ &= -\frac{A'}{A}V' - \frac{\rho_{\mathrm{a}}p}{A}J_m(V) \end{aligned}$$

The general cable equation is then

$$V''(z) + \frac{A'(z)}{A(z)}V' - \frac{\rho_a p(z)}{A(z)}J_m(V,z) = 0 \tag{A.3}$$

This version is ready to be solved using numerical integrations.

But for further analysis, we wish to transform this equation in the form

$$y'' + y = 0 \tag{A.4}$$

First we introduce a non-dimensional length variable $\xi \equiv \frac{z}{\lambda(z)}$ such that

$$\begin{aligned} \frac{d}{dz} &= \frac{1}{\lambda}\frac{d}{d\xi} \\ \frac{d^2}{dz^2} &= \frac{1}{\lambda}\frac{d}{d\xi}\left(\frac{1}{\lambda}\frac{d}{d\xi}\right) \\ &= \frac{1}{\lambda^2}\left(\frac{d^2}{d\xi^2} - \frac{1}{\lambda}\frac{d\lambda}{d\xi}\frac{d}{d\xi}\right). \end{aligned}$$

With this new variable, and introducing a characteristic conductance g for consistency of the units, Equation A.3 becomes:

$$\lambda^{-2}V''(\xi) + \lambda^{-2}\left(\frac{A'(\xi)}{A(\xi)} - \frac{\lambda'(\xi)}{\lambda(\xi)}\right)V'(\xi) - \frac{\rho_{\mathrm{a}}p(\xi)}{A(\xi)}\frac{g(\xi)}{g_o}J_m(V(\xi)) = 0\,.$$

From now on, we assume every function as a function of X instead of x, i.e. a function like $A(x)$ is transformed such that $A(\lambda\xi) \to A(\xi)$ and $\frac{d}{d\xi}A(\lambda\xi) \to A'(\xi)$

We find a nonuniform length scale for the system:

$$\lambda(\xi) = \sqrt{\frac{A(\xi)}{\rho_{\mathrm{a}}g(\xi)p(\xi)}}$$

The cable equation then has the simpler form:

$$V'' + \frac{1}{2}\left(\frac{A'}{A} - \frac{p'}{p} - \frac{g'}{g}\right)V' - \frac{J_m(V)}{g_o} = 0\,. \tag{A.5}$$

We omit the dependence in ξ for readability. New variables varying in ξ will only have their dependency explicitly shown once.

For simplicity, it is useful to redefine A and p as we are modeling the axon, an object mostly cylindrical with a varying radius r. We still allows for some divergence from the perfect cylinder by including a parameter $0 < \kappa(\xi) < 1$ to the cross section area:

$$\begin{aligned} p &= 2\pi r \\ A &= \kappa\pi r^2\,. \end{aligned}$$

The variable κ could be useful to model a bleb or the flower-shaped cross-section of the paranode. The length constant is now written

$$\lambda = \sqrt{\frac{r\kappa}{2\rho_a g_o}}$$

and the cable equation:

$$V'' + u(\xi)V' + \frac{J_m(V)}{g_o} = 0 \tag{A.6}$$

where

$$\begin{aligned} u &= \frac{3}{2}\frac{r'}{r} - \frac{1}{2}\frac{\kappa'}{\kappa} - \frac{1}{2}\frac{g_o'}{g_o} \\ &= \left(\ln\sqrt{\frac{r^3 g}{\kappa}}\right)'\,. \end{aligned}$$

We wish to get rid of the term uV'. We introduce another change of variable to a dimensionless voltage ϕ:

$$\begin{aligned} V &= v(\xi)\phi(\xi) \\ V' &= v'\phi + v\phi' \\ V'' &= v''\phi + 2v'\phi' + v\phi''\,. \end{aligned}$$

The cable equation then expands to:

$$\phi'' + \left(u + 2\frac{v'}{v}\right)\phi' + \left(u\frac{v'}{v} + \frac{v''}{v}\right)\phi - \frac{J_m(v\phi)}{g_o v} = 0\,. \tag{A.7}$$

If we set v such that $u + 2\frac{v'}{v} = 0$, then

$$\begin{aligned} v &= \frac{1}{2}\exp\left(-\int u\, d\xi\right) \\ &= v_o \sqrt[4]{\frac{\kappa g}{r^3}}\,, \end{aligned}$$

with v_o being the appropriate constant of integration. We can finally get rid of the term with first derivative :

$$\begin{aligned} \phi'' + \left(u\left(-\frac{1}{2}u\right) + \left(\frac{1}{2}u' + \frac{1}{4}u^2\right)\right)\phi &= 0 \\ \phi'' + \left(\frac{1}{2}u' - \frac{1}{4}u^2\right)\phi - \frac{J_m(v\phi)}{g_o v} &= 0 \end{aligned}$$

(we used $(\ln a)'' = \left(\frac{a'}{a}\right)' = \frac{a''}{a} - (\frac{a'}{a})^2$). We get the simple equation

$$\phi'' - q\phi + \frac{J_m(V_o\phi)}{g_o V_o} = 0 \tag{A.8}$$

where $q(\xi) = \frac{1}{2}u' + \frac{1}{4}u^2$.

A.1.1 Example : non-uniform conductance

Using a linear but nonuniform conductance $J_m \equiv g(z)V + C\dot{V}$, and setting $g_o = g(x = 0)$ we get the cable equation:

$$\begin{aligned} \phi'' - q\phi - \frac{gv\phi + Cv\dot{\phi}}{g_o v} &= 0 \\ \phi'' - (q + \frac{g}{g_o})\phi + \tau\dot{\phi} &= 0 \end{aligned} \tag{A.9}$$

where τ is $\frac{C}{g_o}$. We see that there's a factor $(q + \frac{g}{g_o})$ with q depending on the geometry of the axon and the axial dependence of g. The solution for this equation when using a delta as an initial condition is:

$$\phi(\xi, t) = \sqrt{\frac{\tau}{2t}} e^{-(q + \frac{g}{g_o})\frac{t}{\tau}} e^{-\frac{\xi^2}{4\frac{t}{\tau}}} \tag{A.10}$$

which shows that the factor $(q + \frac{g}{g_o})$ affects the decay as would an additional conductance. This change in the temporal behaviour would be conserved as the time was kept as is in all our transformations. Furthermore we can find that the maximum of this function does not necessarily stay at the point of injection. If we only allow g to vary, a maximum is found at a z such that

$$\begin{aligned}
\frac{d}{dz}V &= 0 \\
\frac{1}{\lambda}V' &= 0 \\
u'\phi + u\phi' &= 0 \\
\frac{1}{2}\frac{\xi_{\max}(t)}{\frac{t}{\tau}} &= -\frac{u'}{u} \\
\xi_{\max}(t) &= 2\frac{t}{\tau}\left(\frac{g''}{g'} - \frac{g'}{g}\right).
\end{aligned}$$

For a simple, linearly (in ξ-space) increasing distribution of g, it is clear that $\xi_{\max}$ is not zero and progresses in space linearly. To get the maximum in the original space, more work is necessary, and probably no additional insight would result from it:

$$z_{\max} = 2\lambda(z_{\max})^2\frac{t}{\tau}\left(\frac{\frac{d\lambda}{dz}}{\lambda} + \frac{\frac{d^2g}{dz^2}}{\frac{dg}{dz}} - \frac{\frac{dg}{dz}}{g}\right).$$

Now, to see whether this maximum can be amplified, we get the value of V at this maximum, replace in equation A.10 and get:

$$\begin{aligned}
\phi_{\max}(t) &= \sqrt{\frac{\tau}{t}}e^{-\frac{1}{2}\gamma}e^{-(q+\frac{g}{g_o})\frac{t}{\tau}} \\
\phi_{\max}(\xi_{\max}(t)) &= \sqrt{2\frac{\gamma}{\xi_{\max}(t)}}e^{-\frac{1}{2}\gamma}e^{-\frac{1}{2}(q+\frac{g}{g_o})\frac{\xi_{\max}(t)}{\gamma}} \\
V_{\max}(\xi_{\max}(t)) &= V_o\sqrt[4]{g(\xi_{\max}(t))}\sqrt{2\frac{\gamma}{\xi_{\max}(t)}}e^{-\frac{1}{2}\gamma}e^{-\frac{1}{2}(q+\frac{g}{g_o})\frac{\xi_{\max}(t)}{\gamma}}
\end{aligned}$$

where $\gamma = \left(\frac{g''}{g'} - \frac{g'}{g}\right)$. For the right choice of g, $V_{\max}$ is maximal at $t \neq 0$. As in v, r has a $\frac{3}{4}$ exponent instead of $\frac{1}{4}$ as for g, a change in radius has more power to concentrate the voltage away from the injection site than a change in conductance density.

A reminder that so far we only considered a *perfectly ohmic* conductivity. The modification of the decay, and the traveling and amplifying maximum are all effects of geometry.

A.1.2 Example: Effect on threshold

A note on non-ohmic conductance. Take a conductance which includes a threshold $J_m = gV(1 - \frac{V}{V_{\text{th}}})$:

$$\phi'' + q\phi + \frac{gv\phi\left(1 - \frac{v\phi}{V_{\text{th}}}\right)}{g_o v} = 0$$

$$\phi'' + q\phi + \frac{g}{g_o}\left(1 - \frac{\phi}{\frac{V_{\text{th}}}{v}}\right)\phi = 0$$

$$\phi'' + (q + \frac{g}{g_o})\left(1 - \frac{\phi}{\phi_{\text{th}}}\right)\phi = 0$$

where

$$\phi_{\text{th}} = (\frac{g}{g_o} + q)\frac{V_{\text{th}}}{v}$$

is the new threshold with a spatial dependence even if V_{th} didn't have any.

A.1.3 Example: Conical segment

Let's take a segment of axon of length L with a linearly decreasing radius from r_p to r_d:

$$r(z) = r_p + (r_d - r_p)\frac{z}{L}\,. \tag{A.11}$$

This axon has a space constant

$$\begin{aligned}\lambda(z) &= \lambda_p \sqrt{r(z)} r_p \\ &= \lambda_p \sqrt{1 + \left(\frac{r_d}{r_p} - 1\right)\frac{z}{L}}\end{aligned} \tag{A.12}$$

which helps define ξ:

$$\begin{aligned}\xi(z) &= \int_0^z \frac{dz'}{\lambda(z')} \\ &= \int_0^z \frac{dz'}{\lambda_p \sqrt{1 + \left(\frac{r_d}{r_p} - 1\right)\frac{z}{L}}} \\ &= \frac{2}{\left(\frac{r_d}{r_p} - 1\right)}\frac{L}{\lambda_p}\sqrt{1 + \left(\frac{r_d}{r_p} - 1\right)\frac{z}{L}}\end{aligned} \tag{A.13}$$

$$z(\xi) = \lambda_p \xi + \frac{1}{4}\frac{\left(\frac{r_d}{r_p} - 1\right)}{L}\lambda_p^2 \xi^2\,. \tag{A.14}$$

We then rewrite λ and r as functions of ξ:

$$\begin{aligned}\lambda(\xi) &= \lambda_p \sqrt{1 + \left(\frac{r_d}{r_p} - 1\right)\frac{\lambda_p}{L}\xi + \frac{1}{4}\left(\frac{r_d}{r_p} - 1\right)^2 \left(\frac{\lambda_p}{L}\right)^2 \xi^2} \\ &\approx \lambda_p \left(1 + \frac{1}{2}\left(\frac{r_d}{r_p} - 1\right)\frac{\lambda_p}{L}\xi\right) \qquad \text{(A.15)} \\ r(\xi) &= r_p \left(1 + \left(\frac{r_d}{r_p} - 1\right)\frac{\lambda_p}{L}\xi + \frac{1}{4}\left(\frac{r_d}{r_p} - 1\right)^2 \left(\frac{\lambda_p}{L}\right)^2 \xi^2\right) \\ &\approx r_p \left(1 + \left(\frac{r_d}{r_p} - 1\right)\frac{\lambda_p}{L}\xi\right) . \qquad \text{(A.16)}\end{aligned}$$

We finally obtain the normalized variables:

$$u(\xi) \approx \frac{3}{2}\left(\frac{r_d}{r_p} - 1\right)\frac{\lambda_p}{L} \qquad \text{(A.17)}$$

$$q(\xi) \approx \frac{3}{16}\left(\frac{r_d}{r_p} - 1\right)^2 \left(\frac{\lambda_p}{L}\right)^2 \qquad \text{(A.18)}$$

$$v(\xi) = v_o r(\xi)^{-\frac{3}{4}} . \qquad \text{(A.19)}$$

Our numerical simulations in chapter 4 were done using these normalized variables.

Bibliography

[Angelino and Brenner, 2007] Angelino, E. and Brenner, M. P. (2007). Excitability Constraints on Voltage-Gated Sodium Channels. *PLoS Computational Biology (PLOSCB) 8(9)*, 3(9):1751–1760.

[Baalman et al., 2013] Baalman, K. L., Cotton, R. J., Rasband, S. N., and Rasband, M. N. (2013). Blast Wave Exposure Impairs Memory and Decreases Axon Initial Segment Length. *Journal of Neurotrauma*, 30(9):741–751.

[Baloh, 2008] Baloh, R. H. (2008). Mitochondrial Dynamics and Peripheral Neuropathy. *The Neuroscientist*.

[Barnes and Polleux, 2009] Barnes, A. P. and Polleux, F. (2009). Establishment of axon-dendrite polarity in developing neurons. *Annual review of neuroscience*, 32:347–381.

[Berghs et al., 2000] Berghs, S., Aggujaro, D., Dirkx, R., Maksimova, E., Stabach, P., Hermel, J. M., Zhang, J. P., Philbrick, W., Slepnev, V., Ort, T., and Solimena, M. (2000). betaIV spectrin, a new spectrin localized at axon initial segments and nodes of ranvier in the central and peripheral nervous system. *The Journal of cell biology*, 151(5):985–1002.

[Berthold et al., 1993] Berthold, C. H., Fabricius, C., Rydmark, M., and Anders n, B. (1993). Axoplasmic organelles at nodes of Ranvier. I. Occurrence and distribution in large myelinated spinal root axons of the adult cat. *Journal of Neurocytology*, 22(11):925–940.

[Boucher et al., 2012] Boucher, P.-A., Joós, B., and Morris, C. E. (2012). Coupled left-shift of Nav channels: modeling the Na+-loading and dysfunctional excitability of damaged axons. *Journal of Computational Neuroscience*, 33(2):301–319.

[Brette, 2013] Brette, R. (2013). Sharpness of spike initiation in neurons explained by compartmentalization. *PLoS Computational Biology (PLOSCB) 8(9)*, 9(12):e1003338.

[Buffington and Rasband, 2011] Buffington, S. A. and Rasband, M. N. (2011). The axon initial segment in nervous system disease and injury. *The European journal of neuroscience*, 34(10):1609–1619.

[Büki et al., 2000] Büki, A., Okonkwo, D. O., Wang, K. K. W., and Povlishock, J. T. (2000). Cytochrome c Release and Caspase Activation in Traumatic Axonal Injury. *The Journal of ....*

[Cantrell and Catterall, 2001] Cantrell, A. R. and Catterall, W. A. (2001). Neuromodulation of Na+ channels: An unexpected form of cellular platicity. *Nature Reviews Neuroscience*, 2(6):397–407.

[Catterall, 2000] Catterall, W. A. (2000). From ionic currents to molecular mechanisms: The structure and function of voltage-gated sodium channels. *Neuron*, 26(1):13–25.

[Choi and Waxman, 2011] Choi, J.-S. and Waxman, S. G. (2011). Physiological interactions between Na(v)1.7 and Na(v)1.8 sodium channels: a computer simulation study. *Journal of neurophysiology*, 106(6):3173–3184.

[Clark et al., 2009] Clark, B. D., Goldberg, E. M., and Rudy, B. (2009). Electrogenic tuning of the axon initial segment. *The Neuroscientist : a review journal bringing neurobiology, neurology and psychiatry*, 15(6):651–668.

[Debanne et al., 2011] Debanne, D., Campanac, E., Bialowas, A., Carlier, E., and Alcaraz, G. (2011). Axon Physiology. *Physiological Reviews*, 91(2):555–602.

[Dimitrov, 2005] Dimitrov, A. G. (2005). Internodal sodium channels ensure active processes under myelin manifesting in depolarizing afterpotentials. *Journal of Theoretical Biology*, 235(4):451–462.

[Doyle et al., 1998] Doyle, D. A., Cabral, J. M., Pfuetzner, R. A., Kuo, A., Gulbis, J. M., Cohen, S. L., Chait, B. T., and MacKinnon, R. (1998). The structure of the potassium

channel: molecular basis of K+ conduction and selectivity. *Science (New York, N.Y.)*, 280(5360):69–77.

[Fitzhugh, 1962] Fitzhugh, R. (1962). Computation of impulse initiation and saltatory conduction in a myelinated nerve fiber. *Biophysical Journal*, 2:11–21.

[Grubb et al., 2011] Grubb, M. S., Shu, Y., Kuba, H., Rasband, M. N., Wimmer, V. C., and Bender, K. J. (2011). Short- and Long-Term Plasticity at the Axon Initial Segment. *Journal of Neuroscience*, 31(45):16049–16055.

[Hedstrom et al., 2007] Hedstrom, K. L., Xu, X., Ogawa, Y., Frischknecht, R., Seidenbecher, C. I., Shrager, P., and Rasband, M. N. (2007). Neurofascin assembles a specialized extracellular matrix at the axon initial segment. *The Journal of cell biology*, 178(5):875–886.

[Hodgkin and Huxley, 1952a] Hodgkin, A. L. and Huxley, A. F. (1952a). A quantitative description of membrane current and its application to conduction and excitation in nerve. *The Journal of Physiology*, 117(4):500–544.

[Hodgkin and Huxley, 1952b] Hodgkin, A. L. and Huxley, A. F. (1952b). Currents carried by sodium and potassium ions through the membrane of the giant axon of Loligo. *The Journal of Physiology*, 116(4):449–472.

[Hu et al., 2009] Hu, W., Tian, C., Li, T., Yang, M., Hou, H., and Shu, Y. (2009). Distinct contributions of Nav1.6 and Nav1.2 in action potential initiation and backpropagation. *Nature Neuroscience*, 12(8):996–1002.

[Isacoff et al., 1990] Isacoff, E. Y., Jan, Y. N., and Jan, L. Y. (1990). Evidence for the formation of heteromultimeric potassium channels in Xenopus oocytes. *Nature*, 345(6275):530–534.

[Iwata, 2004] Iwata, A. (2004). Traumatic Axonal Injury Induces Proteolytic Cleavage of the Voltage-Gated Sodium Channels Modulated by Tetrodotoxin and Protease Inhibitors. *The Journal of neuroscience : the official journal of the Society for Neuroscience*, 24(19):4605–4613.

[Jack et al., 1975] Jack, J., Noble, D., and Tsien, R. W. (1975). Electric current flow in excitable cells.

[Kole et al., 2008] Kole, M. H. P., Ilschner, S. U., Kampa, B. M., Williams, S. R., Ruben, P. C., and Stuart, G. J. (2008). Action potential generation requires a high sodium channel density in the axon initial segment. *Nature Neuroscience*, 11(2):178–186.

[Kole et al., 2007] Kole, M. H. P., Letzkus, J. J., and Stuart, G. J. (2007). Axon initial segment Kv1 channels control axonal action potential waveform and synaptic efficacy. *Neuron*, 55(4):633–647.

[Kuba, 2010] Kuba, H. (2010). Plasticity at the axon initial segment. *Communicative & integrative biology*, 3(6):597–598.

[Kuba et al., 2006] Kuba, H., Ishii, T. M., and Ohmori, H. (2006). Axonal site of spike initiation enhances auditory coincidence detection. *Nature*, 444(7122):1069–1072.

[Kuba et al., 2010] Kuba, H., Oichi, Y., and Ohmori, H. (2010). Presynaptic activity regulates Na(+) channel distribution at the axon initial segment. *Nature*, 465(7301):1075–1078.

[Lachance et al., 2014] Lachance, M., Longtin, A., Morris, C. E., Yu, N., and Joós, B. (2014). Stimulation-induced ectopicity and propagation windows in model damaged axons. *Journal of Computational Neuroscience*, 37(3):523–531.

[Lai and Jan, 2006] Lai, H. and Jan, L. (2006). The distribution and targeting of neuronal voltage-gated ion channels. *Nature Reviews Neuroscience*, 7(7):548–562.

[Lewis et al., 2005] Lewis, D. A., Hashimoto, T., and Volk, D. W. (2005). Cortical inhibitory neurons and schizophrenia. *Nature Reviews Neuroscience*, 6(4):312–324.

[Li et al., 2006] Li, Y., Um, S. Y., and McDonald, T. V. (2006). Voltage-gated potassium channels: regulation by accessory subunits. *The Neuroscientist : a review journal bringing neurobiology, neurology and psychiatry*, 12(3):199–210.

[Lorincz and Nusser, 2010] Lorincz, A. and Nusser, Z. (2010). Molecular identity of dendritic voltage-gated sodium channels. *Science (New York, N.Y.)*, 328(5980):906–909.

[Mainen et al., 1995] Mainen, Z. F., Joerges, J., Huguenard, J. R., and Sejnowski, T. J. (1995). A model of spike initiation in neocortical pyramidal neurons. *Neuron*, 15(6):1427–1439.

[Martínez-Hernández et al., 2013] Martínez-Hernández, J., Ballesteros-Merino, C., Fernández-Alacid, L., Nicolau, J. C., Aguado, C., and Luján, R. (2013). Polarised localisation of the voltage-gated sodium channel Na(v)1.2 in cerebellar granule cells. *Cerebellum (London, England)*, 12(1):16–26.

[Nakada et al., 2003] Nakada, C., Ritchie, K., Oba, Y., Nakamura, M., Hotta, Y., Iino, R., Kasai, R., Yamaguchi, K., Fujiwara, T., and Kusumi, A. (2003). Accumulation of anchored proteins forms membrane diffusion barriers during neuronal polarization. *Nature Cell Biology*, 5(7):626–U3.

[Naundorf et al., 2006] Naundorf, B., Wolf, F., and Volgushev, M. (2006). Unique features of action potential initiation in cortical neurons. *Nature*, 440(7087):1060–1063.

[Ogawa and Rasband, 2008] Ogawa, Y. and Rasband, M. N. (2008). The functional organization and assembly of the axon initial segment. *Current opinion in neurobiology*, 18(3):307–313.

[Palmer and Stuart, 2006] Palmer, L. M. and Stuart, G. J. (2006). Site of action potential initiation in layer 5 pyramidal neurons. *The Journal of neuroscience : the official journal of the Society for Neuroscience*, 26(6):1854–1863.

[Payandeh et al., 2011] Payandeh, J., Scheuer, T., Zheng, N., and Catterall, W. A. (2011). The crystal structure of a voltage-gated sodium channel. *Nature*, 475(7356):353–358.

[Platkiewicz and Brette, 2010] Platkiewicz, J. J. and Brette, R. R. (2010). A threshold equation for action potential initiation. *Audio, Transactions of the IRE Professional Group on*, 6(7):e1000850–e1000850.

[Rasband, 2010] Rasband, M. N. (2010). The axon initial segment and the maintenance of neuronal polarity. *Nature Reviews Neuroscience*, 11(8):552–562.

[Royeck et al., 2008] Royeck, M. M., Horstmann, M.-T. M., Remy, S. S., Reitze, M. M., Yaari, Y. Y., and Beck, H. H. (2008). Role of axonal NaV1.6 sodium channels in action potential initiation of CA1 pyramidal neurons. *Journal of neurophysiology*, 100(4):2361–2380.

[Ruppersberg et al., 1990] Ruppersberg, J. P., Schröter, K. H., Sakmann, B., Stocker, M., Sewing, S., and Pongs, O. (1990). Heteromultimeric channels formed by rat brain potassium-channel proteins. *Nature*, 345(6275):535–537.

[Rush et al., 2005] Rush, A. M., Dib-Hajj, S. D., and Waxman, S. G. (2005). Electrophysiological properties of two axonal sodium channels, Nav1.2 and Nav1.6, expressed in mouse spinal sensory neurones. *The Journal of Physiology*, 564(Pt 3):803–815.

[Schafer et al., 2009] Schafer, D. P., Jha, S., Liu, F., Akella, T., McCullough, L. D., and Rasband, M. N. (2009). Disruption of the axon initial segment cytoskeleton is a new mechanism for neuronal injury. *The Journal of neuroscience : the official journal of the Society for Neuroscience*, 29(42):13242–13254.

[Sekerli et al., 2004] Sekerli, M., Del Negro, C. A., Lee, R. H., and Butera, R. J. (2004). Estimating action potential thresholds from neuronal time-series: new metrics and evaluation of methodologies. *Biomedical Engineering, IEEE Transactions on*, 51(9):1665–1672.

[Shepherd, 2015] Shepherd, G. M. (2015). *Foundations of the Neuron Doctrine*. Oxford University Press, USA.

[Skulachev, 2001] Skulachev, V. P. (2001). Mitochondrial filaments and clusters as intracellular power-transmitting cables. *Trends in biochemical sciences*.

[Susuki and Rasband, 2008] Susuki, K. and Rasband, M. N. (2008). Spectrin and Ankyrin-Based Cytoskeletons at Polarized Domains in Myelinated Axons. *Experimental Biology and Medicine*.

[Vacher et al., 2008] Vacher, H., Mohapatra, D. P., and Trimmer, J. S. (2008). Localization and targeting of voltage-dependent ion channels in mammalian central neurons. *Physiological Reviews*, 88(4):1407–1447.

[Van Wart et al., 2007] Van Wart, A., Trimmer, J. S., and Matthews, G. (2007). Polarized distribution of ion channels within microdomains of the axon initial segment. *Journal of Comparative Neurology*, 500(2):339–352.

[Verkman, 2013] Verkman, A. S. (2013). Diffusion in the extracellular space in brain and tumors. *Physical Biology*, 10(4):045003.

[Wang et al., 2009] Wang, J. A., Lin, W., Morris, T., Banderali, U., Juranka, P. F., and Morris, C. E. (2009). Membrane trauma and Na+ leak from Nav1.6 channels. *American Journal of Physiology - Cell Physiology*, 297(4):C823–C834.

[Wang et al., 2008] Wang, S. S.-H. S., Shultz, J. R. J., Burish, M. J. M., Harrison, K. H. K., Hof, P. R. P., Towns, L. C. L., Wagers, M. W. M., and Wyatt, K. D. K. (2008). Functional trade-offs in white matter axonal scaling. *Journal of Neuroscience*, 28(15):4047–4056.

[Yu and Catterall, 2003] Yu, F. H. and Catterall, W. A. (2003). Overview of the voltage-gated sodium channel family. *Genome biology*, 4(3):207.

[Yu et al., 2012] Yu, N., Morris, C. E., Joós, B., and Longtin, A. (2012). Spontaneous Excitation Patterns Computed for Axons with Injury-like Impairments of Sodium Channels and Na/K Pumps. *PLoS Computational Biology (PLOSCB) 8(9)*, 8(9):e1002664.

[Zonta et al., 2011] Zonta, B., Desmazieres, A., Rinaldi, A., Tait, S., Sherman, D. L., Nolan, M. F., and Brophy, P. J. (2011). A critical role for Neurofascin in regulating action potential initiation through maintenance of the axon initial segment. *Neuron*, 69(5):945–956.